

AD-A173 132

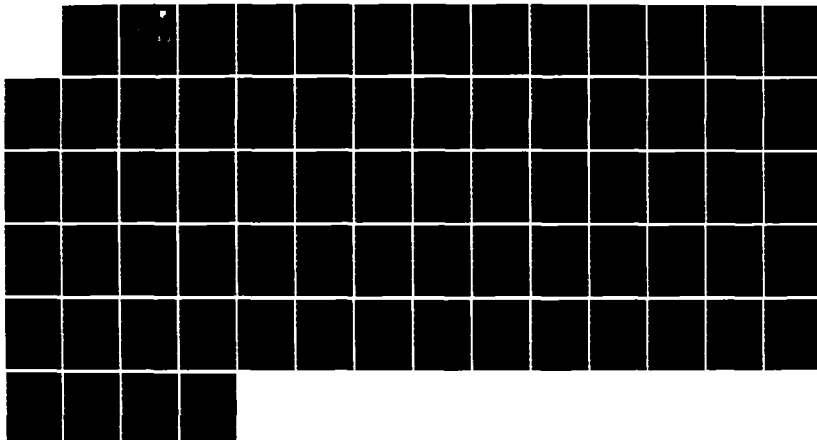
THEORY OF VHF SCATTERING BY FIELD-ALIGNED
IRREGULARITIES IN THE IONOSPHERE(U) SIGMATRON INC
LEXINGTON MA A MALAGA SEP 86 A447-12 RADC-TR-86-118
F19628-84-C-0117

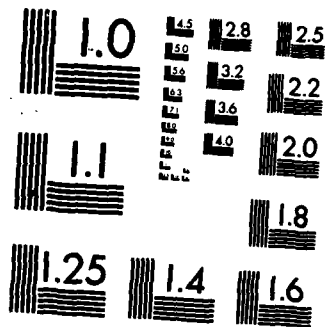
1/1

UNCLASSIFIED

F/G 20/14

NL





MICROCOPY RESOLUTION TEST CHART
NATIONAL BUREAU OF STANDARDS-1963-A

AD-A173 132

RADC-TR-86-118
Interim Report
September 1986

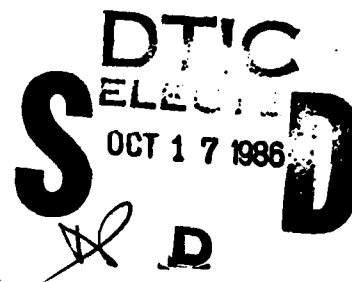


12

***THEORY OF VHF SCATTERING BY
FIELD-ALIGNED IRREGULARITIES
IN THE IONOSPHERE***

Signatron, Inc.

Alfonso Malaga



APPROVED FOR PUBLIC RELEASE; DISTRIBUTION UNLIMITED

DTIC FILE COPY

**ROME AIR DEVELOPMENT CENTER
Air Force Systems Command
Griffiss Air Force Base, NY 13441-5700**

This report has been reviewed by the RADC Public Affairs Office (PA) and is releasable to the National Technical Information Service (NTIS). At NTIS it will be releasable to the general public, including foreign nations.

RADC-TR-86-118 has been reviewed and is approved for publication.

APPROVED:



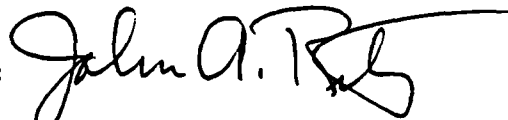
MICHAEL J. SOWA
Project Engineer

APPROVED:



ALLAN C. SCHELL
Chief
Electromagnetic Sciences Division

FOR THE COMMANDER:



JOHN A. RITZ
Plans & Programs Division

If your address has changed or if you wish to be removed from the RADC mailing list, or if the addressee is no longer employed by your organization, please notify RADC (EEPS) Hanscom AFB MA 01731-5000. This will assist us in maintaining a current mailing list.

Do not return copies of this report unless contractual obligations or notices on a specific document requires that it be returned.

UNCLASSIFIED

SECURITY CLASSIFICATION OF THIS PAGE

AD-A173132

REPORT DOCUMENTATION PAGE

1a. REPORT SECURITY CLASSIFICATION UNCLASSIFIED			1b. RESTRICTIVE MARKINGS N/A		
2a. SECURITY CLASSIFICATION AUTHORITY N/A			3. DISTRIBUTION / AVAILABILITY OF REPORT Approved for public release; distribution unlimited.		
2b. DECLASSIFICATION / DOWNGRADING SCHEDULE N/A			5. MONITORING ORGANIZATION REPORT NUMBER(S) RADC-TR-86-118		
4. PERFORMING ORGANIZATION REPORT NUMBER(S) A447-12			7a. NAME OF MONITORING ORGANIZATION Rome Air Development Center (EEPS)		
6a. NAME OF PERFORMING ORGANIZATION Signatron, Inc.		6b. OFFICE SYMBOL (if applicable)		7b. ADDRESS (City, State, and ZIP Code) Hanscom AFB MA 01731-5000	
6c. ADDRESS (City, State, and ZIP Code) 110 Hartwell Avenue Lexington MA 02173			9. PROCUREMENT INSTRUMENT IDENTIFICATION NUMBER F19628-84-C-0117		
8a. NAME OF FUNDING / SPONSORING ORGANIZATION Rome Air Development Center		8b. OFFICE SYMBOL (if applicable) EEPS		10. SOURCE OF FUNDING NUMBERS	
8c. ADDRESS (City, State, and ZIP Code) Hanscom AFB MA 01731-5000			PROGRAM ELEMENT NO. 62702F	PROJECT NO. 4600	TASK NO. 16
11. TITLE (Include Security Classification) THEORY OF VHF SCATTERING BY FIELD-ALIGNED IRREGULARITIES IN THE IONOSPHERE					
12. PERSONAL AUTHOR(S) Alfonso Malaga					
13a. TYPE OF REPORT Interim		13b. TIME COVERED FROM Jun 84 TO Aug 85		14. DATE OF REPORT (Year, Month, Day) September 1986	
15. PAGE COUNT 76					
16. SUPPLEMENTARY NOTATION N/A					
17. COSATI CODES			18. SUBJECT TERMS (Continue on reverse if necessary and identify by block number)		
FIELD 17	GROUP 02	SUB-GROUP 1	Field Aligned Scatter, Anisotropic Scatter		
20	14		Auroral Scatter VHF Propagation		
19. ABSTRACT (Continue on reverse if necessary and identify by block number) The theory which describes the scattering of VHF radiowaves by anisotropic irregularities aligned along the earth's magnetic field is presented and applied to treat auroral scatter. Results which show the aspect sensitivity, polarization effects, antenna bandwidth effects and frequency dependence of auroral scatter are presented.					
20. DISTRIBUTION / AVAILABILITY OF ABSTRACT <input type="checkbox"/> UNCLASSIFIED/UNLIMITED <input checked="" type="checkbox"/> SAME AS RPT. <input type="checkbox"/> DTIC USERS			21. ABSTRACT SECURITY CLASSIFICATION UNCLASSIFIED		
22a. NAME OF RESPONSIBLE INDIVIDUAL Michael J. Sowa			22b. TELEPHONE (Include Area Code) (617) 861-4266		22c. OFFICE SYMBOL RADC (EEPS)

DD FORM 1473, 84 MAR

83 APR edition may be used until exhausted.
All other editions are obsolete.SECURITY CLASSIFICATION OF THIS PAGE
UNCLASSIFIED

TABLE OF CONTENTS

<u>SECTION</u>	<u>PAGE</u>
1 INTRODUCTION	1
2 THEORY OF FIELD-ALIGNED SCATTER.....	2
2.1 SPECULAR SCATTER CONDITIONS.....	4
2.2 ANISOTROPIC SCATTERING THEORY.....	12
2.2.1 Calculation of Direction of Magnetic Field Line.....	19
2.2.2 Calculation of the Direction Cosines and Scattering Angle.....	22
2.2.3 Calculation of Average Scattered Power....	25
2.2.4 Calculation of RMS Delay Spread.....	31
3 AURORAL SCATTER RESULTS.....	32
3.1 ASPECT SENSITIVITY OF AURORAL SCATTER.....	35
3.2 POLARIZATION CONSIDERATIONS.....	37
3.3 ANTENNA BEAMWIDTH EFFECTS.....	41
3.4 FREQUENCY DEPENDENCE.....	45
4 SUMMARY AND CONCLUSIONS.....	45

APPENDIX A POLARIZATION EFFECTS IN FIELD-ALIGNED SCATTER



Accession For	
NTIS CRA&I	<input checked="" type="checkbox"/>
DTIC TAB	<input type="checkbox"/>
Unannounced	<input type="checkbox"/>
Justification	
By	
Distribution /	
Availability Codes	
Dist	Avail and/or Special
A-1	

LIST OF FIGURES

<u>FIGURE</u>		<u>PAGE</u>
1	Geometry for Specular Scatter.....	6
2	Locus of Receiver Locations where Specular Reflections from Indicated E-layer Scatterer Locations Can Be Received Due to a Transmitter at T_x	10
3	Locus of Receiver Locations where Specular Reflections from Indicated F-layer Scatterer Locations Can Be Received Due to a Transmitter at T_x	11
4	Field-aligned Scattering Geometry.....	17
5	Geometry for Calculation of the Earth's Magnetic Field Lines	20
6	Polar Isonosphere Features as a Function of Latitude and Local Time	33
7	Contours of Constant Relative Path Loss in dB.....	36
8	Contours of Constant Delay Spread in Microseconds.....	38
9	Geometry for Calculation of Antenna Pattern Effects...	44

LIST OF TABLES

<u>TABLES</u>	<u>PAGE</u>
1 Polarization Effects at 45 MHz.....	40
2 Antenna Azimuth Beamwidth Effects at 45 MHz.....	43
3 Frequency Effects.....	46

THEORY OF VHF SCATTERING BY FIELD-ALIGNED IRREGULARITIES IN THE IONOSPHERE

1. INTRODUCTION

Long range propagation of Very High Frequency (VHF) radio-waves via scattering from ionospheric irregularities is of importance to the design of Meteor Burst Communications Systems for the following reasons: i) it can be used as a means to communicate at distances of a few hundred kilometers in the absence of meteor trails provided the communications waveform can cope with the 'distortions' introduced by the propagation medium; and ii) when present along with meteor trails, it can interfere with the meteor scatter signal. In either case, it is important to know the conditions under which scattering from ionospheric irregularities will occur, the strength of the scattered signal and other parameters such as the coherence bandwidth or delay spread and the coherence time or Doppler spread.

Scattering from ionospheric irregularities can in principle occur almost anywhere on earth. However, it has been most frequently observed at high latitudes [Collins and Forsyth, 1959] and near the equator [Ferguson, 1981] while very weak signals have been reported at mid-latitudes [Bailey et al., 1955]. The reason for this is that the scattering of VHF radiowaves at high latitudes is associated with the radio-aurora which produces irregular ionization at E-layer heights in the ionosphere. The scattering phenomenon is known as auroral scatter. The equatorial observations are associated with nighttime field-aligned irregularities in the ionization of the F-region of the ionosphere. Because the phenomenology of the high-latitude radio-aurora emulates that of a nuclear burst disturbed ionosphere, strong scattering from field-aligned irregularities at VHF can also be expected to occur at lower latitudes after a high-altitude (100-500 km) nuclear burst.

In Section 2 of this report we develop a theory for VHF scattering by field-aligned ionospheric irregularities which describes the conditions under which such phenomena occurs. Results which illustrate the geometrical (aspect) sensitivity of the scattering by field-aligned irregularities at E-layer heights (90-140 km) in the auroral region are presented in Section 3. The theory developed is very general, though, and also applies to scattering by field-aligned irregularities induced by high-altitude nuclear bursts at arbitrary latitudes. The main difference between auroral scatter and scattering at lower latitudes is that at high latitudes only energy scattered by irregularities in the E-layer (90-140 km heights) can be received by a terminal on the surface of the earth. Energy scattered by irregularities in the ionization of the F-layer (200-500 km) does not intersect the surface of the earth because of the directionality caused by the anisotropy of field-aligned irregularities. At lower latitudes field-aligned irregularities in the E and F-regions contribute to the total received scattered field. However, the scattering cross-section of the irregularities in the F-layer is greater than that of the E-layer irregularities so that, at lower latitudes, most of the received energy is due to F-layer irregularities.

In addition to the aspect sensitivity (geometry) of field-aligned scatterer we also present in Section 3 results which illustrate polarization effects, antenna height, pointing and beamwidth effects, and frequency dependence. The theory needed to determine polarization effects is discussed in Appendix A.

2. THEORY OF FIELD-ALIGNED SCATTER

The scattering of VHF radiowaves by field-aligned irregularities of ionization in the ionosphere has been treated in the literature as specular scatter [Stathacopoulos and Barry, 1974] or as scatter from long cylindrical irregularities whose ratio of length to diameter is large [Booker, 1956].

The specular scatter theory predicts the reception of a scattered signal only in those regions where the specular condition (to be defined later) is satisfied. This restricts the areas of the world in which field-aligned scatter would be observed for a given scattering volume. For example according to the specular scatter theory, scattering from irregularities at an altitude of 250 km or higher (F-layer scattering) should only be observed when the ground based transmitters and receivers are located at geomagnetic latitudes below 40° . Similarly scattering from irregularities at altitudes less than 120 km (E-layer irregularities) should occur only when the transmitter and receiver are at geomagnetic latitudes below 62° . However there is experimental evidence that shows that scattering from the radio-aurora can be observed in the neighborhood of the auroral zone (geomagnetic latitudes between 67° and 73° under undisturbed conditions), and sometimes even north of it where the specular condition cannot be satisfied [Collins and Forsyth, 1959]. On the other hand, there is also evidence that the scattered signal is stronger and can be observed more often in areas where the specular condition is approached. This type of behavior is predicted when the irregularities are modeled as cylinders whose longitudinal dimension is at least four times greater than their diameter and such that their axis are aligned with the earth's magnetic field. This is essentially the theory of anisotropic scattering proposed by Booker [1956] to explain observations of scattering from the radio-aurora.

In this section we will develop a model for calculating and predicting the path loss of anisotropic scatter given the geographic locations of the transmitter and receiver, and the height and geographic region of the scattering volume where the field-aligned irregularities are contained. Since the scatter from anisotropic irregularities is aspect sensitive, it is always useful to know the receiving locations where the specular scatter

condition is satisfied. Therefore we begin with a derivation of the specular scatter condition.

2.1 SPECULAR SCATTER CONDITIONS

In many instances it may be necessary to determine locations where specular scatter from field aligned irregularities may be expected given the location of the transmitter and the scatterer.

The condition for specular scatter from elongated irregularities is that the component of the scattered wave vector, \hat{u}_0 , parallel to the longitudinal axis of the irregularity, \hat{u}_f , be equal to the component of incident wave vector, \hat{u}_i , parallel to the longitudinal axis of the irregularity, i.e.,

$$\hat{u}_0 \cdot \hat{u}_f = \hat{u}_i \cdot \hat{u}_f \quad (1)$$

where $\hat{a} \cdot \hat{b}$ is the 'dot product' between vectors \hat{a} and \hat{b} , and

$$\hat{u}_i = (\bar{P} - \bar{T})/R_t = \text{unit vector from transmitter at } \bar{T} \text{ to scatterer at } \bar{P}.$$

$$\hat{u}_0 = (\bar{R} - \bar{P})/R_r = \text{unit vector from scatterer at } \bar{P} \text{ to receiver at } \bar{R}.$$

$$\hat{u}_f = \text{unit vector parallel to earth's magnetic field at the scattering point } \bar{P}.$$

The incident wave vector \hat{u}_i can be decomposed into a component parallel to \hat{u}_f and perpendicular to \hat{u}_f

as

$$\hat{u}_i = \cos \alpha \hat{u}_f + \sin \alpha \hat{u}_N \quad (2)$$

where

$$\cos \alpha = \hat{u}_i \cdot \hat{u}_f \quad (3)$$

The angle of incidence α is also referred to as the aspect angle.

The specular scattered wave vector \hat{u}_0 can then be expressed as

$$\hat{u}_0 = \cos \alpha \hat{u}_f + \sin \alpha \cos \beta \hat{u}_N + \sin \alpha \sin \beta (\hat{u}_f \times \hat{u}_N) \quad (4)$$

where $-\pi < \beta < \pi$, i.e., specular scatter due to an elongated irregularity is possible within a cone defined by the angles α and β . Figure 1 shows two typical scattered rays which intersect the earth at possible receiver sites \bar{R}_1 and \bar{R}_2 . The locus of all such intersection points defines a curve on the surface of the earth where strong scattered signals can be received. Field-aligned scatterers are, of course, not concentrated at a point, as implied in Figure 1; however the coverage provided by many distributed scatterers may be calculated by summing the contributions from each. We will now describe how to find the locus of scattered rays which intersect the surface of the earth given the geomagnetic latitude, θ_t , and geomagnetic longitude, ϕ_t , of the transmitter, and the altitude, h , geomagnetic latitude θ , and geomagnetic longitude, ϕ , of the scatterer.

Define a cartesian coordinate system such that the transmitter location is given by $\bar{T} = a(\cos \theta_t \cos \phi_t, \cos \theta_t \sin \phi_t, \sin \theta_t)$ and the scatterer location by $\bar{P} = r(\cos \theta \cos \phi, \cos \theta \sin \phi, \sin \theta)$ where a is the radius of the earth and $r = a + h$. We want to determine the geomagnetic latitude, θ_r , and longitude, ϕ_r , of all locations \bar{R} which satisfy the specular scatter conditions (1)-(4) such that $|\bar{R}| = a$, i.e., we want to find all specular scattered

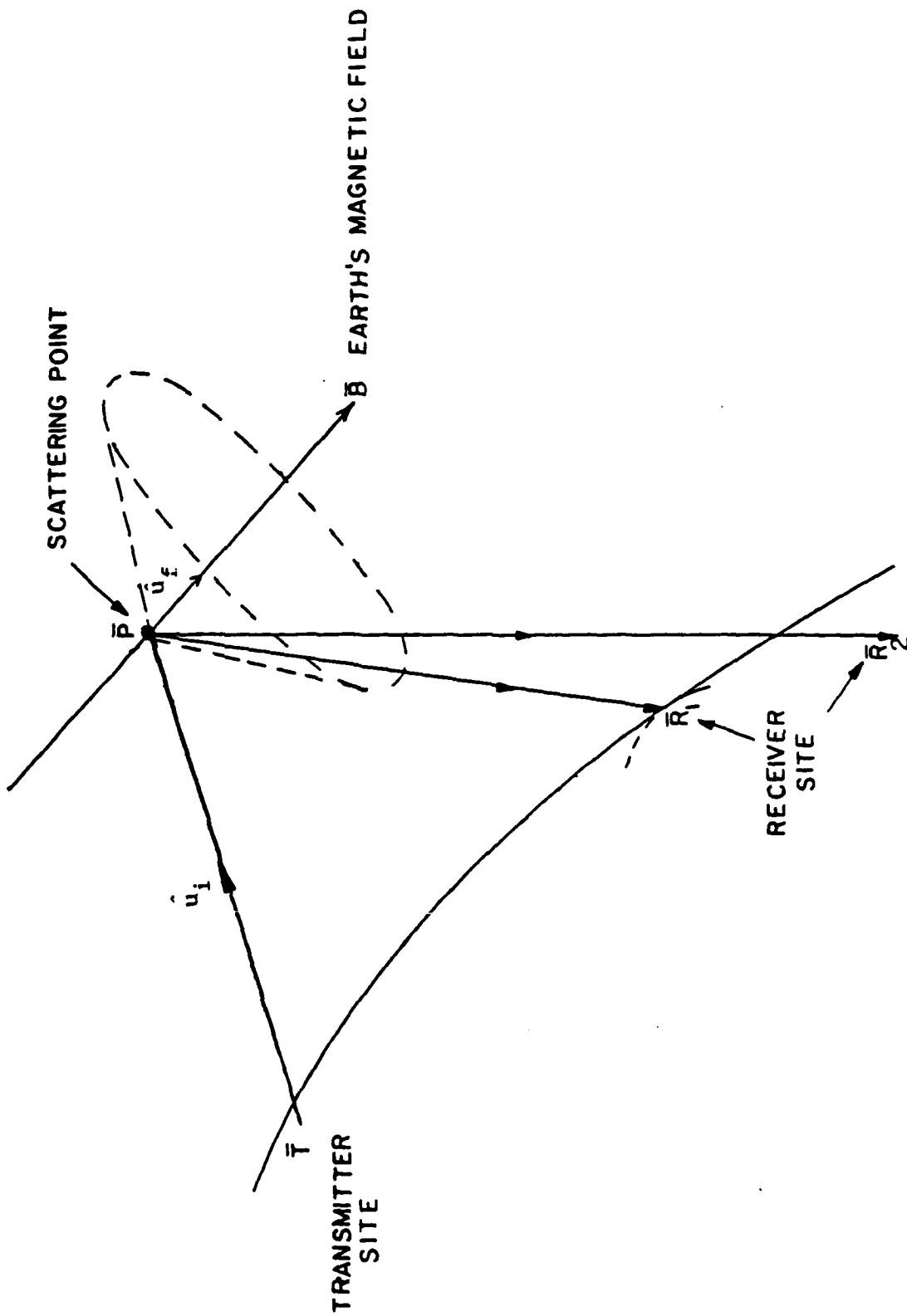


Figure 1 Geometry for Specular Scatter

rays which intersect the surface of the earth. We will assume that the incident and scattered rays propagate in straight lines so that the results are only applicable at VHF where ray bending in the E-layer of the ionosphere is negligible.

From the definition of the scattered ray equation

$$\bar{D} = \bar{P} + d \hat{u}_0(\alpha, \beta) \quad (5)$$

where \bar{D} is the location of a point at a distance d from the scattering point, we can first find the distance d_0 along the scattered ray at which the ray is closest to the center of the earth as follows.

The square of the distance from the center of the earth to a location \bar{D} on the scattered ray is given by

$$D^2(d) = \bar{D} \cdot \bar{D} = \bar{P} \cdot \bar{P} + 2d\bar{P} \cdot \hat{u}_0 + d^2 \quad (6)$$

The shortest distance from the center of the earth to a point along the ray $\bar{D}(d)$ occurs at the point d_0 where the first derivative of Equation (6) with respect to d is equal to zero, i.e.,

$$0 = 2 \bar{P} \cdot \hat{u}_0(\alpha, \beta) + 2d_0 \quad (7)$$

and $D_0 = D(d_0)$ is given by

$$D_0^2(\alpha, \beta) = \bar{P} \cdot \bar{P} - [\bar{P} \cdot \hat{u}_0(\alpha, \beta)]^2 \quad (8)$$

If $D_0^2 < a^2$ and $d_0 > 0$ then the scattered ray intersects the surface of the earth. The receiving locations where the rays (parameterized by α and β) intersect the surface of the earth are those that satisfy

$$a^2 = \bar{P} \cdot \bar{P} + 2 R_r \bar{P} \cdot \hat{u}_0(\alpha, \beta) + R_r^2 \quad (9)$$

where $R_r = |\bar{P} - \bar{R}|$ is the distance between the scatterer at \bar{P} and the specular receive location at \bar{R} . This distance is given by

$$R_r(\alpha, \beta) = -\bar{P} \cdot \hat{u}_0(\alpha, \beta) - \sqrt{a^2 - D_0^2(\alpha, \beta)} \quad (10)$$

provided $\bar{P} \cdot \hat{u}_0 < 0$, and $D_0^2(\alpha, \beta) < a^2$.

The receive locations (α, β) satisfying (10) are

$$\begin{aligned} \bar{R}(\alpha, \beta) &= \bar{P} + R_r(\alpha, \beta) \hat{u}_0(\alpha, \beta) \\ &= a(\cos \theta_r \cos \phi_r, \cos \theta_r \sin \phi_r, \sin \theta_r) \end{aligned} \quad (11)$$

where the geomagnetic latitude, θ_r , and longitude, ϕ_r , are found from

$$\tan \theta_r = \frac{P_z + R_r u_z}{\sqrt{(P_x + R_r u_x)^2 + (P_y + R_r u_y)^2}} \quad (12)$$

$$\tan \phi_r = \frac{P_y + R_r u_y}{P_x + R_r u_x} \quad (13)$$

with $\hat{u}_0 = (u_x, u_y, u_t)$.

Figure 2 shows the locus of all specular receive locations for a transmitter located at geographic latitude of 61°N and longitude 150°W (near Anchorage, Alaska) and a few scatterers at an altitude of 110 km height (E-layer) at geographic latitudes and longitudes which are within the auroral oval (say at geomagnetic latitudes of 65°N, 67°N and 69°N). Rays (radiowaves) scattered by irregularities at geomagnetic latitudes greater than 71°N and 110 km altitude do not intersect the surface of the earth. Similarly rays scattered by irregularities at 220 km or higher (F-layer) and geomagnetic latitudes coinciding with the auroral oval do not intersect the surface of the earth either. If the transmitter location is moved to a location at a geographic latitude of 65°N and longitude of 148°W (near Fairbanks, Alaska) then none of the rays scattered by E-layer or F-layer irregularities within the auroral oval intersect the surface of the earth. This implies that specular scatter from irregularities within the auroral oval should not be observable at Fairbanks, Alaska.

For comparison purposes we show in Figure 3 the locus of all specular receive locations for a transmitter located at geographic latitude of 35°N and longitude 120°W (geomagnetic latitude of 41.7°N) and scatterers at an altitude of 250 km (F-layer) at the geographic locations shown and which correspond to geomagnetic latitudes between 46°N and 56°N. The scatterers may be irregularities in the ionization of the F-layer occurring as a result of a high-altitude nuclear burst. Rays scattered by

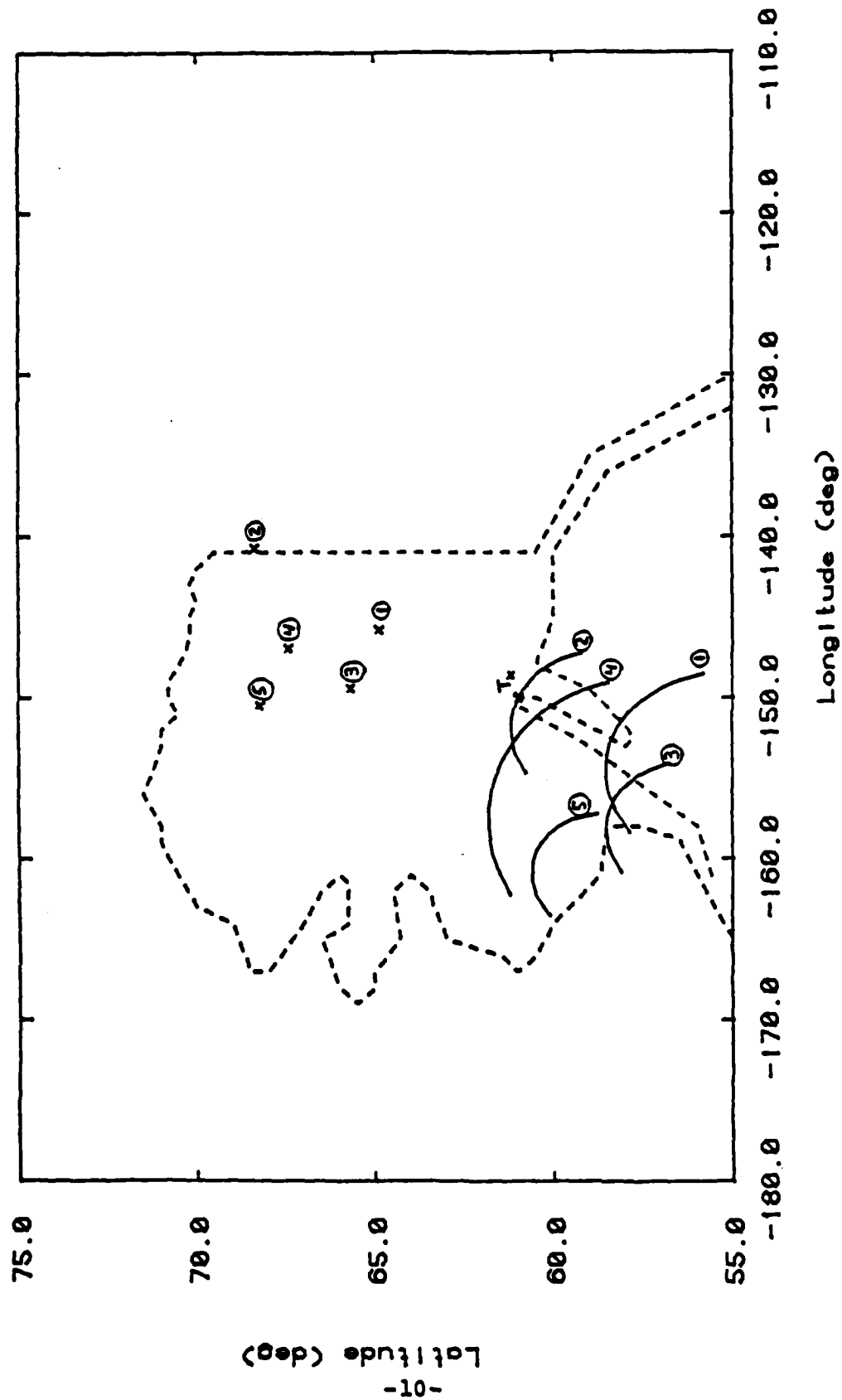


Figure 2 Locus of receiver locations (solid lines) where specular reflections from indicated E-layer scatterer locations (x's) can be received due to a transmitter at T_x

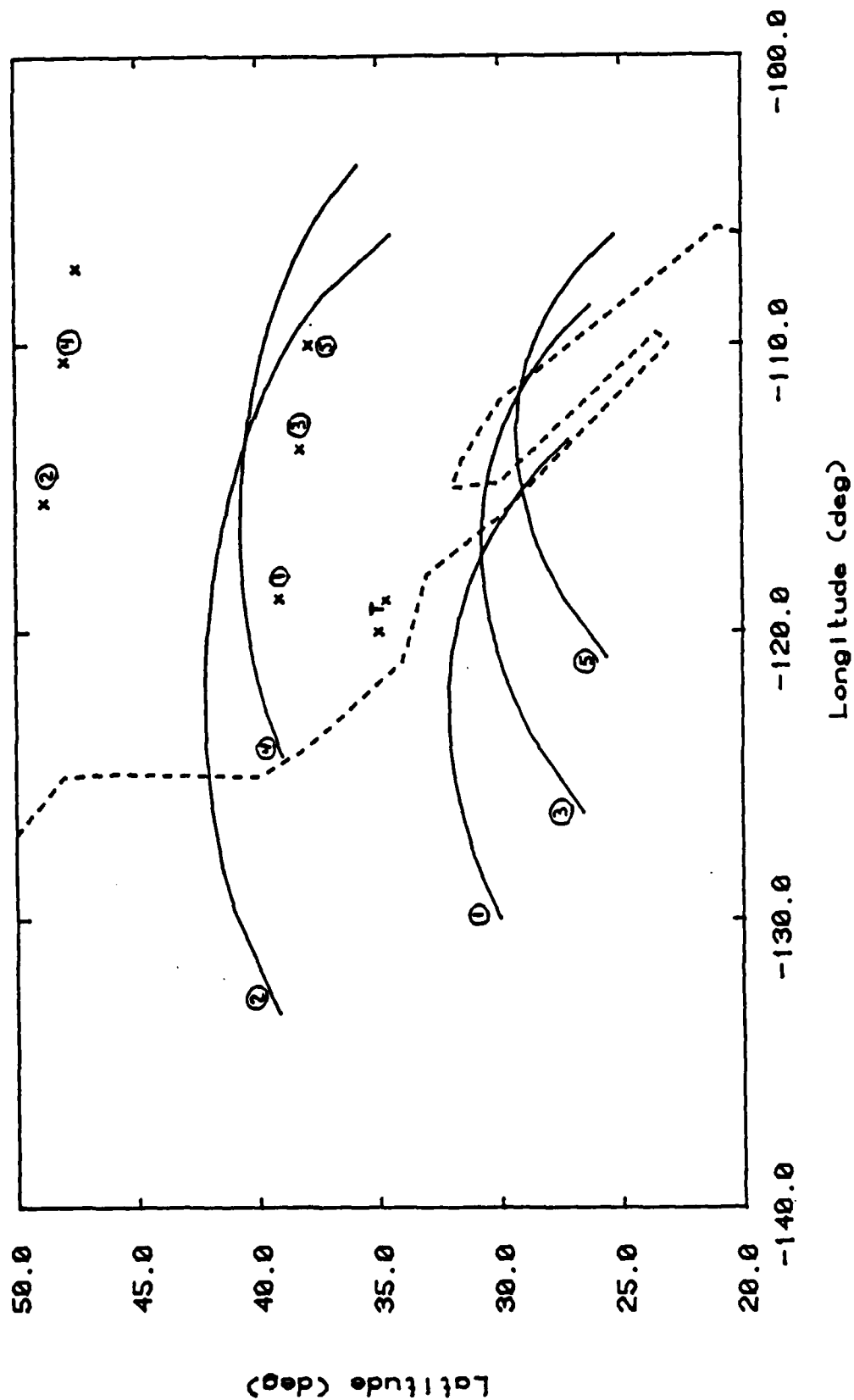


Figure 3 Locus of receiver locations (solid lines) where specular reflections from indicated F-layer scatterer locations (x's) can be received due to a transmitter at T_x

irregularities at geomagnetic latitudes below 44°N do not intersect the surface of the earth.

The two examples of Figures 2 and 3 indicate that even at mid-latitudes, both transmitter and receiver must be at least 4° of latitude south (in geomagnetic coordinates) of the scattering region in order for the specular condition to be satisfied. This condition can be relaxed somewhat when one takes into account that the scatter from field-aligned irregularities is not purely specular. We discuss the theory of scattering by anisotropic field-aligned irregularities next.

2.2 ANISOTROPIC SCATTERING THEORY

Auroral scatter at VHF is a phenomenon by which energy is scattered by elongated irregularities which are aligned with the earth's magnetic field. The irregularities are random perturbations in the refractive index of the medium caused by random fluctuations in the electron density at heights between 100 km and 500 km above the earth's surface. Because the irregularities are elongated, the random fluctuations in the refractive index are anisotropic. Field aligned scatter from ionospheric irregularities also occurs at night at equatorial latitudes and elsewhere after a nuclear explosion has occurred at ionospheric heights. This latter case is often referred to as the 'bomb mode' of propagation.

The total received power can be expressed as

$$P_r = P_t G_t G_r \frac{\lambda^2}{(4\pi)^2} \iiint_V e^{-0.23K_A} \frac{\sigma d^3r}{R_t^2 R_r^2} \quad (14)$$

where σ is the scattering cross-section per unit volume of the irregularities, R_t is the distance from the transmitter to the

scatterer, R_r is the distance from the scatterer to the receiver, K_A is the two-way absorption loss incurred as the incident and scattered waves propagate through the D-region of the ionosphere and the integration is over the portion of the scattering region intersected by the transmit and receive antenna beams. Note that the scattering cross-section per unit volume, σ , differs from the radar backscatter cross-section, by a factor of 4π .

If we assume that each scattered wave undergoes single-scattering within the scattering volume, the scattering cross-section of the field-aligned irregularities is given by

$$\sigma = \frac{1}{(2\pi)^2} k^4 \sin^2 \chi \overline{\Delta n^2} S[k(\ell_2 - \ell_1), k(m_2 - m_1), k(n_2 - n_1)] \quad (15)$$

where

χ = angle between incident E vector and the direction of scattering

k = $2\pi/\lambda$

$\overline{\Delta n^2}$ = refractive index variance due to presence of field-aligned irregularities in the ionosphere

$S(\cdot)$ = normalized (unity refractive index variance) three-dimensional wavenumber spectrum of the refractive index fluctuations defined later in Equation (19) This normalization implies

$$\iiint S(k_x, k_y, k_z) dk_x dk_y dk_z = (2\pi)^3 .$$

\hat{u}_1 = (ℓ_1, m_1, n_1) = direction cosines of incident wave vector.

\hat{u}_0 = (ℓ_2, m_2, n_2) = direction cosines of scattered wave vector.

The single-scattering assumption used in arriving at (15) is valid for most cases of interest including auroral scatter. However in some nuclear-disturbed ionospheric scatter channels it may be necessary to include multiple scattering effects. In this case the scattering cross-section is given by (15) with the normalized wavenumber spectrum $S(\cdot)$ replaced by an 'effective' wavenumber spectrum which includes Fresnel diffraction effects and multiple-scattering effects [Yang and Yeh, 1984]. Multiple-scattering has the net effect of reducing the forward scattered power ($\hat{u}_i = \hat{u}_0$) and enlarging the cone of angles where significant power is scattered. The results presented in this report will be based on the single-scattering assumption.

The refractive index variance can be expressed in terms of the electron density fluctuations by noting that the refractive index in the ionosphere is given by

$$\begin{aligned}
 n &= \sqrt{1 - \frac{b_0(N+\Delta N)}{f^2}} \\
 &= \sqrt{1 - \frac{f_N^2}{f^2}} - \frac{1}{2} \frac{f_N^2/f^2}{1 - \frac{f_N^2}{f^2}} \left(\frac{\Delta N}{N} \right)
 \end{aligned} \tag{16}$$

where

- N = mean electron density
- ΔN = perturbation in electron density due to field aligned irregularities
- f_N = $\sqrt{b_0 N}$ plasma frequency of ionosphere (varies with height)
- f = frequency
- b_0 = $e^2/4\pi^2\epsilon_0 m$, e is the electron charge, m is its mass and ϵ_0 is the free space permittivity.

The peak plasma frequency of the ionosphere occurs at the height of maximum ionization in the F2 layer and is less than 15 MHz so that at VHF $f^2 \gg f_N^2$.^{*} The refractive index variance is then approximately given by

$$\overline{\Delta n^2} = \frac{1}{4} \frac{f_N^4}{f^4} \overline{\left(\frac{\Delta N}{N}\right)^2} \quad (17)$$

The scattering cross-section of the irregularities can then be expressed as

$$\sigma = \pi^2 \left[\frac{f_N(z)}{c} \right]^4 \sin^2 \chi \overline{\left(\frac{\Delta N}{N}\right)^2} S[k(\hat{u}_2 - \hat{u}_1)] \quad (18)$$

where c is the speed of light. The normalized wavenumber spectrum is defined as

$$S(\bar{K}) = \iiint B_n(\bar{r}) e^{j\bar{K} \cdot \bar{r}} d^3\bar{r} \quad (19)$$

where $B_n(\cdot)$ is the normalized spatial correlation of the electron density fluctuations. In the case of field-aligned irregularities with cylindrical symmetry, we assume (19) can be written as

$$\begin{aligned} S(K_T, K_L) &= \iiint B_T(r_T) B_L(r_L) e^{j(\bar{K}_T \cdot \bar{r}_T + \bar{K}_L \cdot \bar{r}_L)} d^2\bar{r}_T d\bar{r}_L \\ &= S_T(K_T) S_L(K_L) \end{aligned} \quad (20)$$

* NOTE: This also allows us to neglect ray bending effects at VHF due to the background electron density.

where $S_T(\cdot)$ is referred to as the two-dimensional transverse wavenumber spectrum of the irregularities and $S_L(\cdot)$ is the longitudinal wavenumber spectrum.

This expression assumes that the spatial correlation of the electron density fluctuations is separable. One such example is one in which the irregularities are uniform along the magnetic field so that the random fluctuations occur in the plane perpendicular to the magnetic field only. In general, the correlation distance of the field-aligned irregularities will be much greater along the magnetic field lines. Thus, the scattering cross-section of the field-aligned irregularities is of the form

$$\sigma = \pi^2 \left(\frac{f_N}{c}\right)^4 \sin^2 \chi \left(\frac{\Delta N}{N}\right)^2 S_T[k \sqrt{(m_2 - m_1)^2 + (n_2 - n_1)^2}] S_L[k(l_2 - l_1)]. \quad (21)$$

The problem is then reduced to one of determining the direction cosines in the planes along and perpendicular to the earth's magnetic field.

Using the geometry of Figure 4, the direction cosines can be expressed as

$$(l_2 - l_1) = 2 \sin\left(\frac{\phi_s}{2}\right) \cos \psi \quad (22a)$$

$$[(m_2 - m_1)^2 + (n_2 - n_1)^2]^{1/2} = 2 \sin(\frac{\phi_s}{2}) \sin \psi \quad (22b)$$

where ϕ_s is the scattering angle and ψ is the angle between the longitudinal axis of the irregularities (magnetic field line) and the bisector of the incident and scattered wave sectors.

Equations (22a) and (22b) are arrived at by noting that the scattering angle ϕ_s is defined as

$$\begin{aligned} |\hat{u}_0 - \hat{u}_i|^2 &= (\hat{u}_0 - \hat{u}_i) \cdot (\hat{u}_0 - \hat{u}_i) \\ &= 2 - 2 \hat{u}_0 \cdot \hat{u}_i \\ &= 2(1 - \cos \phi_s) \\ &= 4 \sin^2 \frac{\phi_s}{2} \end{aligned} \quad (23)$$

where \hat{u}_i is a unit vector in direction of the incident wave, \hat{u}_0 is a unit vector in the direction of the scattered wave and ϕ_s is the angle between these two vectors.

The bisector of the incident and scattered wave vectors is the vector $\hat{u}_0 - \hat{u}_i$ shown in Figure 4. The angle that the bisector makes with the magnetic field line is ψ . Therefore the magnitude of the projection of the vector $\hat{u}_0 - \hat{u}_i$ onto the field line is the direction cosine for the longitudinal component of the scattered wave, i.e.,

$$l_2 - l_1 = |\hat{u}_2 - \hat{u}_1| \cos \psi \quad (24a)$$

from which Equation (22a) follows. Equation (22b) follows from the fact that

$$(m_2 - m_1)^2 + (n_2 - n_1)^2 = |u_2 - u_1|^2 - (l_2 - l_1)^2 \quad (24b)$$

Up to this point, the theory of field-aligned scatter is very general. We will now discuss a particular way (model) of calculating the direction cosines based on the use of geomagnetic coordinates as the reference coordinate system and modeling the earth's magnetic field as the dipole field of a sphere. The model could eventually be refined by using corrected geomagnetic coordinates and by including higher order terms for the earth's magnetic field. We have chosen to use the simpler model because it is relatively easy to develop and it contains the features which are relevant to the theory of field-aligned scatter. Addition of the refinements would be appropriate if and when a need to predict accurately the path loss and other parameters of field-aligned scatter for specific geographic locations.

2.2.1 Calculation of Direction of Magnetic Field Line

The calculation of the scattering angle for a given geometry requires knowledge of the orientation of the elongated irregularities. The longitudinal axis of the irregularity coincides with the earth's magnetic field lines. Modeling the earth's magnetic field as a dipole, as shown in Figure 5, we can express the line which passes through a height r at latitude θ as

$$f(r, \theta) = \frac{\cos^2 \theta}{r} = \text{constant} \quad (25)$$

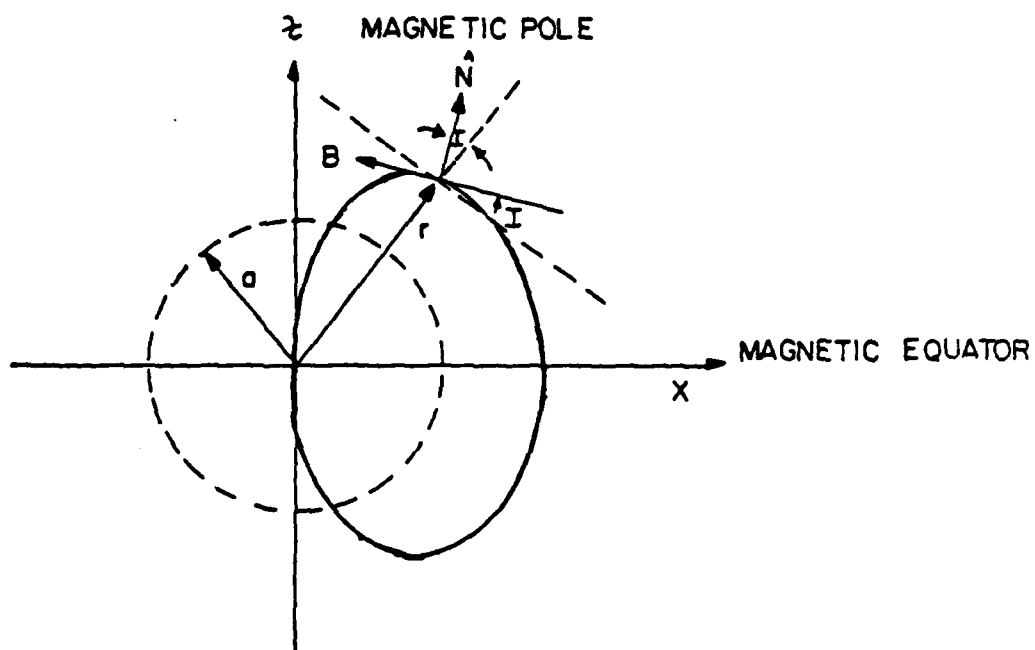


Figure 5 Geometry for Calculation of the Earth's Magnetic Field Lines

where $h=r-a$ is the height of the magnetic field line (irregularity) above the surface of the earth.

In a Cartesian coordinate system, where the x -axis is on the magnetic equator plane and the z -axis passes through the magnetic north pole, the constant field lines can be expressed as

$$f(x, z) = \frac{x^2}{(x^2 + z^2)^{3/2}} \quad (26)$$

If we define \hat{u}_f as a unit vector tangential to the magnetic field line at a given latitude θ and longitude $\phi = 0$, then

$$\begin{aligned} \hat{u}_f &= \left(-\frac{\partial f}{\partial z} \hat{x} + \frac{\partial f}{\partial x} \hat{z} \right) / \left[\left(\frac{\partial f}{\partial x} \right)^2 + \left(\frac{\partial f}{\partial z} \right)^2 \right]^{1/2} \\ &= [3xz \hat{x} + (2z^2 - x^2) \hat{z}] / (x^2 + z^2)^{1/2} (x^2 + 4z^2)^{1/2} \\ &= (1 + 3 \sin^2 \theta)^{-1/2} \{ 3 \cos \theta \sin \theta \hat{x} + (3 \sin^2 \theta - 1) \hat{z} \} \end{aligned} \quad (27)$$

The magnetic field is parallel to the earth's surface at the equator ($\theta=0$), while at the magnetic pole ($\theta=90^\circ$), the magnetic field line is normal to the earth's surface, as expected.

The unit vector parallel to the magnetic field line at arbitrary longitude ϕ is found by rotating the above vector about the z -axis by an angle ϕ so that

$$\hat{u}_f = (1+3 \sin^2 \theta)^{1/2} \{ 3 \cos \theta \sin \theta \cos \phi \hat{x} + 3 \cos \theta \sin \theta \sin \phi \hat{y} \\ + (3 \sin^2 \theta - 1) \hat{z} \}$$

(28)

where the \hat{x} , \hat{y} and \hat{z} axes are as shown in Figure 4. Note that \hat{u}_f is independent of r .

2.2.2 Calculation of the Direction Cosines and Scattering Angle

Let the transmitter be located at geomagnetic latitude and longitude (θ_t, ϕ_t) and the receiver at geomagnetic latitude and longitude (θ_r, ϕ_r) both on the surface of the earth, i.e., $r = a$. Let the scatterer at geomagnetic latitude and longitude (θ, ϕ) be at a height h above the surface of the earth, i.e., $r = a + h$.

The unit vector \hat{u}_i directed from the transmitter to the scatterer can be expressed in the cartesian coordinate system of Figure 4 as

$$\hat{u}_i = \frac{1}{R_t} \{ (r \cos \theta \cos \phi - a \cos \theta_t \cos \phi_t) \hat{x} \\ + (r \cos \theta \sin \phi - a \cos \theta_t \sin \phi_t) \hat{y} \\ + (r \sin \theta - a \sin \theta_t) \hat{z} \} \quad (29)$$

where

$$R_t^2 = r^2 + a^2 - 2ar \cos \alpha_t \quad (30)$$

$$\cos \alpha_t = \sin \theta_t \sin \theta + \cos \theta_t \cos \theta \cos(\phi_t - \phi) \quad (31)$$

The unit vector \hat{u}_0 directed from the scatterer to the receiver is similarly given by

$$\begin{aligned}\hat{u}_0 = & \frac{-1}{R_r} \{ (r \cos \theta \cos \phi - a \cos \theta_r \cos \phi_r) \hat{x} \\ & + (r \cos \theta \sin \phi - a \cos \theta_r \sin \phi_r) \hat{y} \\ & + (r \sin \theta - a \sin \theta_r) \hat{z} \} \quad (32)\end{aligned}$$

where

$$R_r^2 = r^2 + a^2 - 2ar \cos \alpha_r \quad (33)$$

$$\cos \alpha_r = \sin \theta_r \sin \theta + \cos \theta_r \cos \theta \cos(\phi_r - \phi) \quad (34)$$

The longitudinal direction cosine can be determined by noting that

$$\begin{aligned}l_2 - l_1 &= (\hat{u}_0 - \hat{u}_i) \cdot \hat{u}_f \\ &= R_r^{-1} (1 + 3 \sin^2 \theta)^{-1/2} \{-2r \sin \theta + 3a \cos \theta \sin \theta \cos \theta_r \cos(\phi_r - \phi) \\ &\quad + a(3 \sin^2 \theta - 1) \sin \theta_r\} + R_t^{-1} (1 + 3 \sin^2 \theta)^{-1/2} \{-2r \sin \theta \\ &\quad + 3a \cos \theta \sin \theta \cos \theta_t \cos(\phi_t - \phi) + a(3 \sin^2 \theta - 1) \sin \theta_t\} \quad (35)\end{aligned}$$

which after some algebra reduces to

$$\begin{aligned}
 v_L &= l_2 - l_1 = 2 \sin(\phi_s/2) \cos \psi \\
 &= (1 + 3 \sin^2 \theta)^{-1/2} \left\{ 3a \sin \theta \left(\frac{\cos \alpha_t}{R_t} + \frac{\cos \alpha_r}{R_r} \right) \right. \\
 &\quad \left. - 2r \sin \theta \left(\frac{1}{R_t} + \frac{1}{R_r} \right) - a \left(\frac{\sin \theta_t}{R_t} + \frac{\sin \theta_r}{R_r} \right) \right\} \quad (37)
 \end{aligned}$$

The scattering angle, ϕ_s , can be found from its definition

$$\begin{aligned}
 v^2 &= |\hat{u}_1 - \hat{u}_2|^2 = 4 \sin^2(\phi_s/2) \\
 &= \left[r \cos \theta \cos \phi \left(\frac{1}{R_t} + \frac{1}{R_r} \right) - a \left(\frac{\cos \theta_t \cos \phi_t}{R_t} + \frac{\cos \theta_r \cos \phi_r}{R_r} \right) \right]^2 \\
 &\quad + \left[r \cos \theta \sin \phi \left(\frac{1}{R_t} + \frac{1}{R_r} \right) - a \left(\frac{\cos \theta_t \sin \phi_t}{R_t} + \frac{\cos \theta_r \sin \phi_r}{R_r} \right) \right]^2 \\
 &\quad + \left[r \sin \theta \left(\frac{1}{R_t} + \frac{1}{R_r} \right) - a \left(\frac{\sin \theta_t}{R_r} + \frac{\sin \theta_r}{R_r} \right) \right]^2 \quad (38)
 \end{aligned}$$

After some algebra (38) reduces to

$$v^2 = \frac{(R_t + R_r)^2 - 2a^2(1 - \cos \alpha)}{R_t R_r} \quad (39)$$

where

$$\cos \alpha = \sin \theta_t \sin \theta_r + \cos \theta_t \cos \theta_r \cos(\phi_t - \phi_r) \quad (40)$$

The tangential component of the direction cosines can then be calculated from

$$\begin{aligned} v_T^2 &= (m_2 - m_1)^2 + (n_2 - n_1)^2 = 4 \sin^2(\phi_s/2) \cos^2 \psi \\ &= v^2 - v_L^2 \end{aligned} \quad (41)$$

where v is given by Equation (39) and v_L is given by Equation (37).

2.2.3 Calculation of Average Scattered Power

Field-aligned scatter is caused by irregularities which are confined to a range of latitudes and heights above the surface of the earth. This is certainly the case where auroral scatter is concerned as the auroral region occurs at geomagnetic latitudes between 65° and 71° North in the night sector and between 70° and 75° in the day sector under mildly disturbed magnetic conditions. During periods of high magnetic activity the aurora moves southward and during periods of very quiet magnetic activity it moves north by 1 or 2 degrees [Gassmann, 1973]. Field aligned scatter caused by a nuclear explosion at ionospheric heights will on the other hand occur over a wide geographic area which may be equal to a significant portion of the continental US.

Since the scattering region is confined to specific geographic areas, it is convenient to express the scattering integral in (14) in geomagnetic coordinates as

$$P_r = P_t G_t G_r \left(\frac{\lambda}{4\pi}\right)^2 \int_{h_1}^{h_2} dh \int_{\phi_1}^{\phi_2} d\phi \int_{\theta_1}^{\theta_2} d\theta e^{-0.23K_A}$$

$$\frac{g_t(h, \theta, \phi) g_r(h, \theta, \phi) B(h) S_T(h, \theta, \phi) S_L(h, \theta, \phi) r^2 \cos \theta}{R_t^2(h, \theta, \phi) R_r^2(h, \theta, \phi)}$$

(42)

where $h = r - a$ is the height of the scatterer above the surface of the earth, $S_T(\cdot)$ and $S_L(\cdot)$ are the wavenumber spectra of the irregularities in the planes transverse and along the magnetic field, the factor $B(z)$ is proportional to the density of scatterers as a function of height and is defined as

$$B(h) = \pi^2 \left[\frac{f_N(h)}{c} \right]^4 \sin^2 \chi \left(\frac{\Delta N}{N} \right)^2$$

(43)

g_t and g_r are the antenna patterns, h_1 and h_2 are the heights of the bottom and top of the scattering region (e.g., E-layer at high latitudes and F-layer at low and mid latitudes), θ_1 and θ_2 are the geomagnetic latitudes of the southern and northern boundaries of the scattering region (e.g., auroral oval) and ϕ_1 and ϕ_2 are the geomagnetic longitudes over which scattering takes place.

The outer scale of the irregularities along the magnetic field lines is long compared to the wavelength so that the spatial correlation of the electron density fluctuations along the magnetic field lines can be assumed to be Gaussian and

$$S_L(K_L) = \sqrt{2\pi} L \exp\{-(K_L L)^2/2\} \quad (44)$$

where L is the longitudinal outer scale of the irregularities and

$$K_L = 2k \sin \frac{\phi}{2} \cos \psi = kV_L(h, \theta, \phi) \quad (45)$$

with $V_L(h, \theta, \phi)$ given by Equation (37). Specular scatter occurs when $kL \gg 1$ and $V_L = 0$. Note that we have normalized S_L so that $\int S_L(k) dk = 2\pi$.

The wavenumber spectrum in the plane perpendicular to the irregularities is of the form

$$\begin{aligned} S_T(K_T) &= C_m [1 + (K_T L_T)^2]^{-m/2} \\ &= C_m (K_T L_T)^{-m} \end{aligned} \quad (46)$$

where L_T is the outer scale of the irregularities in the plane transverse to the magnetic field, m is wavenumber spectrum slope which determines the frequency dependence of the scattered field, and

$$K_T = 2k \sin \frac{\phi}{2} \sin \psi = kV_T(h, \theta, \phi) \quad (47)$$

with $V_T(h, \theta, \phi)$ given by Equation (41).

The proportionality constant C_m is chosen so that

$$\frac{1}{2\pi} \int_0^\infty dK_T K_T S_T(K_T) = 1 \quad (48)$$

$$\text{i.e., } C_m = 2\pi L_T^2 (m-2), \quad m > 2$$

The density of scatterers per unit height is proportional to the plasma frequency whose height variation can be modeled as

$$\begin{aligned} f_N(h) &= f_{0E} [1 - (h - h_E)^2 / b_E^2]^{1/2}, & h_E - b_E < h < h_E + b_E \\ f_N(h) &= f_{0F} [1 - (h - h_F)^2 / b_F^2]^{1/2}, & h_F - b_F < h < h_F + b_F \end{aligned} \quad (49)$$

where f_{0E} and f_{0F} are the critical frequencies of the E and F layers, h_E and h_F are their heights and b_E and b_F are their half-widths. The critical frequencies, f_{0E} and f_{0F} , exhibit diurnal, seasonal, solar cycle and at high-latitudes magnetic disturbance dependence.

Substituting Equations (43) through (49) in the scattering volume integral (42), we can express the average scattered power as

$$\begin{aligned} P_r &= P_t G_t G_r \left(\frac{c}{2\pi f} \right)^{m-2} \left\{ \left(\frac{f_{0E}}{f} \right)^4 e^{-0.23K_E} C_E^2(m) I(h_E, b_E) \right. \\ &\quad \left. + \left(\frac{f_{0F}}{f} \right)^4 e^{-0.23K_F} C_F^2(m) I(h_F, b_F) \right\} / 16\sqrt{2\pi} \end{aligned} \quad (50)$$

where

$$C_E^2(m) = (m-2)L L_T^{2-m} \overline{\left(\frac{\Delta N}{N} \right)_E^2} \quad (51)$$

$$C_F^2(m) = (m-2)L L_T^{2-m} \overline{\left(\frac{\Delta N}{N} \right)_F^2} \quad (52)$$

$$I(h_0, b) = \int_{h_0-b}^{h_0+b} dh (h+a)^2 \left[1 - \left(\frac{h-h_0}{b} \right)^2 \right]^2 \int_{\phi_1}^{\phi_2} d\phi \int_{\theta_1}^{\theta_2} d\theta \frac{g_t g_r \cos \theta \sin^2 \chi e^{-(kLV_L)^2/2}}{R_t^2 R_r^2 V_T^m}$$

(53)

In arriving at (50)-(53) we have assumed that the critical frequency of the scattering layer, f_0E and f_0F , and the normalized electron density fluctuations are constant within the scattering region. We have also assumed that all rays scattered from irregularities in the E-layer suffer roughly the same absorption loss K_E while all rays scattered from irregularities in the F-layer suffer an absorption loss of K_F dB. These assumptions could be relaxed by including the absorption of each individual scattered ray and the critical frequencies and electron density fluctuations in the integrand of Equation (53).

In arriving at Equation (53) it has also been assumed that the transverse outer scale of the irregularities L_T is much larger than the wavelength of interest so that $KV_T L_T \gg 1$. The two terms in (37) are proportional to the power scattered by irregularities in the E-region (90-150 km) and F-region (150-500 km) of the ionosphere, respectively. The triple integrals $I(h_E, b_E)$ and $I(h_F, b_F)$ depend only on the geometry and polarization of the transmit and receive antennas and can be evaluated given the geographic location of the terminals and the scattering region. Prediction of the scattered power requires modeling of the critical frequencies of the layers, f_0E and f_0F , the absorption loss for E-layer and F-layer scattering, K_E and K_F , and the structure parameters of the irregularities, C_E^2 and C_F^2 . Models of the diurnal, seasonal sunspot and geographical variations of the critical frequencies of the layers and the absorption loss are readily available. The structure parameters depend on the electron density fluctuations, $(\Delta N/N)^2$, the longitudinal and transverse outer scales of the irregularities, L and L_T respec-

tively, and the transverse wavenumber spectrum slope, m . The latter can be determined from the frequency dependence of the scattered power, $f^{-(m+2)}$. A model for the structure parameter $C_N^2(m)$ for field-aligned irregularities in the F-region has been developed by Fremouw and Lansinger [1981] from satellite scintillation data at latitudes ranging from equatorial to high-latitude auroral paths. However it is not clear whether this model applies to ground based terminals. Furthermore when the terminals are on the ground the field-aligned scatter at high latitudes is due to irregularities at E-region heights even though the scattering cross-section (density) of the irregularities at F-layer heights is greater. The reason for this is that the magnetic field lines are nearly vertical at high latitudes and since the scatter due to elongated irregularities is nearly specular, it was shown in Section 2.1 that the energy scattered by F-region irregularities at high latitudes is scattered up and not back towards the earth.

From measurement of the average scattered power on a high latitude (auroral) scatter path we can determine the structure parameter $C_N^2(m)$ for E-region irregularities provided that we can measure independently the absorption loss K_E and the critical frequency of the E-layer, f_{0E} , in the scattering region. The validity of the assumption that field aligned scatter at high latitudes is due to E-region irregularities could possibly be determined from measurement of the delay power impulse response. If both E-region and F-region scatter occur, then the delay power impulse response should exhibit two peaks corresponding to the delay of the energy scattered by irregularities near the maxima of the two layers.

The model of Equations (50)-(53) can also be used to predict the strength of field-aligned scatter due to ionization irregularities caused by a high-altitude nuclear explosion. To do this, it would be necessary to determine the geographical loca-

tion of the nuclear explosion, the rms electron density fluctuations, the mean electron density or plasma frequency of the background ionization after the explosion, the outer scales of the irregularities along and transverse to the magnetic field lines, and the D-region two-way absorption loss. Computer codes which predict these parameters are described in the classified literature.

2.2.4 Calculation of RMS Delay Spread

In addition to the strength of field-aligned scatter, it is of interest to determine the coherence bandwidth or delay spread of the scattered signal. The rms delay spread can be calculated by noting that the delay τ of a scatterer at a distance R_t and R_r from the transmitter and receiver respectively is given by

$$\tau = \frac{R_t + R_r}{c} \quad (54)$$

where c is the propagation velocity.

Then we can define the delay moments of the scattered field as

$$\frac{\tau^n}{n} = \frac{\iiint_v \left(\frac{R_t + R_r}{c} \right)^n \frac{\sigma \exp\{-0.23 K_A\} d^3\vec{r}}{R_t^2 R_r^2}}{\iiint_v \frac{\sigma \exp\{-0.23 K_A\} d^3\vec{r}}{R_t^2 R_r^2}} \quad (55)$$

where σ is the scattering cross-section per unit volume of the irregularities defined in previous sections and the integration is over the scattering volume as outlined in Section 2.2.4.

The rms delay spread is now defined as

$$T_M = 2 \sqrt{\overline{\tau^2} - (\overline{\tau})^2} \quad (56a)$$

and the coherence bandwidth is then defined by

$$B_C = \frac{1}{\pi T_M} \quad (56b)$$

3. AURORAL SCATTER RESULTS

In this section we apply the theoretical model developed in Section 2 to investigate the characteristics of VHF anisotropic scattering by field-aligned irregularities in the auroral E-layer. In particular we will determine the aspect sensitivity of anisotropic scatter, the effects of polarization, antenna height and beamwidth and frequency dependence.

In order to determine these effects we need to establish the location of the auroral E-layer which coincides with the location of the auroral oval. Figure 6 shows the location of the auroral oval (solid lines) in (corrected) geomagnetic coordinates* under quiet magnetic activity when the magnetic index $K_p = 1$. The auroral oval encircles the geomagnetic pole at a constant geomagnetic latitude during the day and moves southward at night. The southern boundary of the auroral oval also moves southward as the magnetic index increases (1° per integer increase in K_p).

* NOTE: The geomagnetic north pole has been assumed to be at latitude 78.3°N and longitude 69°W .

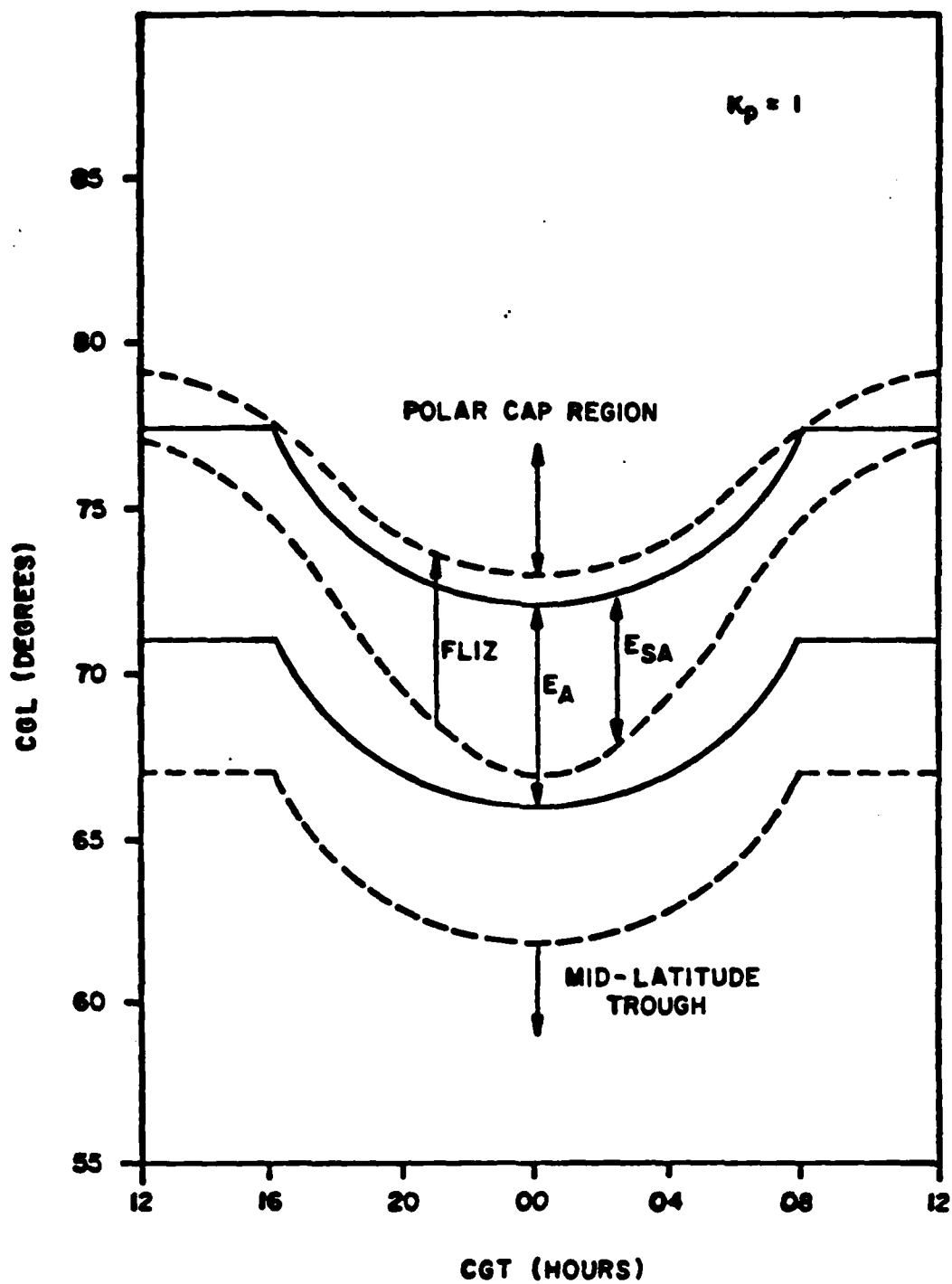


Figure 6 Polar ionosphere features as a function of latitude and local time

The ionization in the E-layer in the auroral region is due to two sources: one is electromagnetic solar radiation and the other is precipitating electrons. The latter is present all the time and is the source of the so called auroral E-layer. Electromagnetic solar radiation produces ionization in those parts of the ionosphere that are illuminated by the sun. Hence it only produces ionization in the day sector. The critical frequency of the E-layer can then be expressed in terms of the contributions from the two sources of ionization as [Gassmann, 1973]

$$f_0E = \left[(f_0E)_{uv}^4 + (f_0E)_A^4 \right]^{1/4} \quad (57)$$

where $(f_0E)_{uv}$ is due to ionization caused by the solar illumination and is a function of geographic location, time-of-day, season, and sunspot number, while $(f_0E)_A$ is due to precipitating electrons in the auroral oval and is a function of the magnetic index. A model for predicting $(f_0E)_{uv}$ given the geographic location, time, month and sunspot number is described by Malaga [1981], while Gassmann [1973] has developed a model for predicting $(f_0E)_A$ as a function of the magnetic activity as measured by the magnetic index K_p . Both of these models have been combined according to Equation (56) to predict the critical frequency of the auroral E-layer, f_0E .

In the remainder of this section we present the results of calculations of the relative path loss of auroral scatter for different conditions. The total path loss, L_T , is defined as

$$L_T = \frac{P_r}{P_t G_t G_r} = \frac{L_r}{C_E^2 \exp(-0.23 K_E)} \quad (58)$$

where L_r is the relative path loss which accounts for all propagation effects except for absorption loss K_E and the unknown structure parameter C_E of the field-aligned irregularities.

3.1 ASPECT SENSITIVITY OF AURORAL SCATTER

Contour plots of constant relative path loss are shown in Figure 7 as a function of geographic coordinates for the case in which the operating frequency is 45 MHz and the transmitter is at a geographic latitude of 61°N and longitude of 150°W (Anchorage, Alaska). The calculations assume antennas with broad azimuth beamwidths and horizontal polarization. The effects of the antenna heights on the elevation pattern are included, however. The antenna heights assumed are 4 meters which result in a broad elevation beamwidth with a null at near grazing elevation angles.

The magnetic index, K_p , assumed was 2 which places the auroral oval at geomagnetic latitudes between 65°N and 71°N during the night. The critical frequency of the E-layer was $f_{0E} = 3.87$ MHz. The height of maximum ionization was 115 km and the bottom and top of the layer were at a height of 90 km and 140 km, respectively. The field-aligned irregularities were assumed to have a longitudinal outer scale (i.e., outer scale along the magnetic field lines) of 10 km which results in fairly aspect-sensitive scatter. Longer outer scales result in even more aspect sensitivity, as the scatter becomes more specular the greater the ratio of longitudinal outer scale to wavelength is. Smaller outer scales result in more isotropic scatter.

These results should be compared with those of Figure 2 where purely specular scatter was assumed. The contour plots of Figure 7 indicate that it is possible to observe auroral scatter in regions where the specular condition is not satisfied, although these signals are much weaker than in those regions where the specular condition is satisfied for a large number of scat-

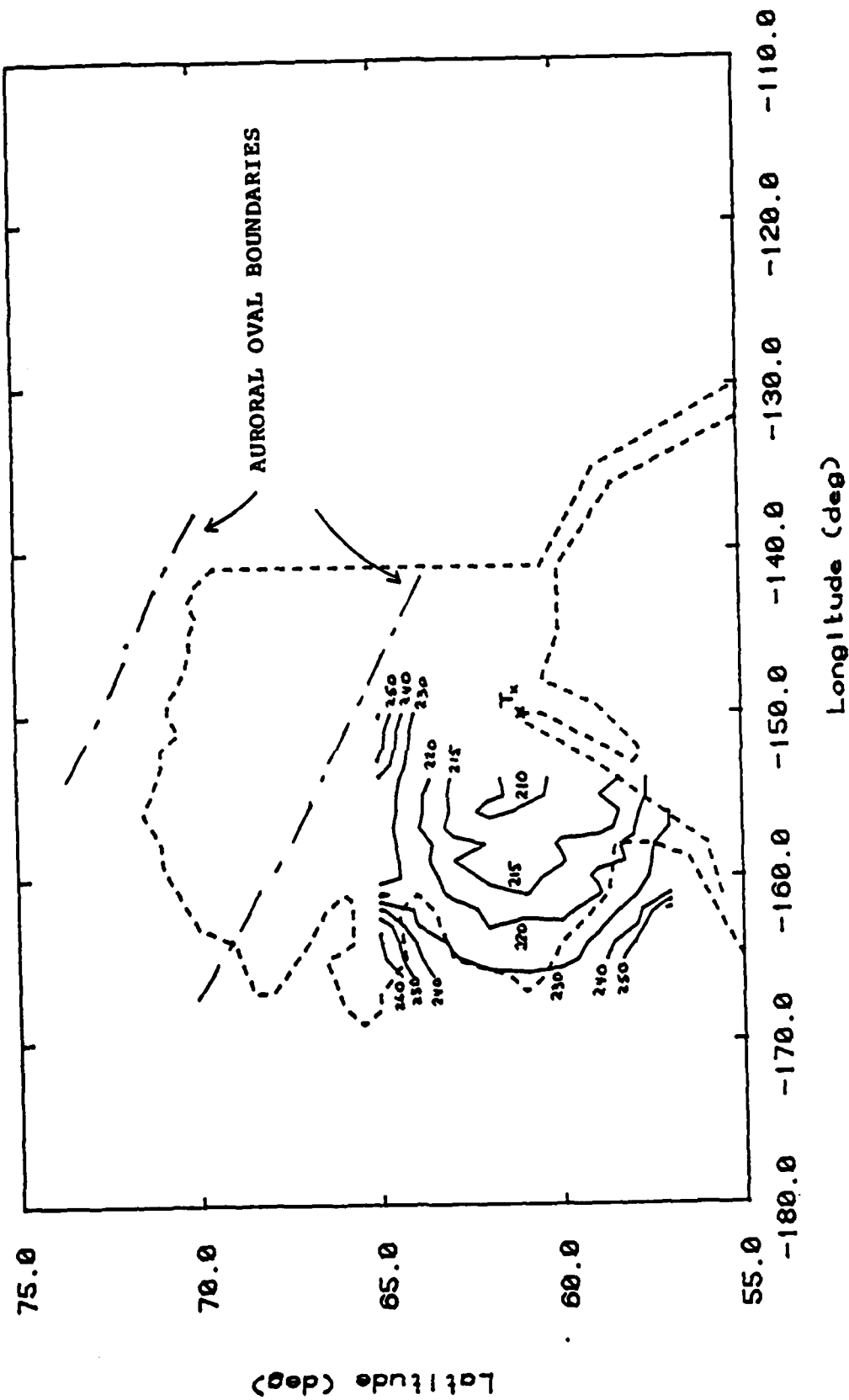


Figure 7 Contours of constant relative path loss in dB

terers. The contour plots also show that the areas where auroral scatter should be observed is still limited geographically due to the anisotropy of the field-aligned irregularities. The size of the area where auroral scatter is observable depends on the degree of anisotropy (longitudinal outer scale). Note that stronger signals are received at locations due west of the transmitter. However scatter signals can still be observed on north-south paths provided both terminals are south of the auroral region.

Figure 8 shows contour plots of the delay spread of the received scattered field in microseconds. The delay spread, which is a measure of the coherence bandwidth, increases as the volume of 'significant' scatterers increases, i.e., scatterers which result in near specular scatter for fixed transmit and receive locations.

3.2 POLARIZATION CONSIDERATIONS

The strength of the auroral scatter signal depends on the polarization on two accounts: i) the $\sin^2\chi$ factor in the volume integral of Equation (53) where χ is the angle between the polarization vector of the wave incident on a scatterer and the direction of the scattered wave, and ii) the effects of ground reflections on the elevation pattern for different antenna polarizations.

In Appendix A, we derive the calculation of the polarization factor $\sin^2\chi$ for different combinations of transmit and receive polarization. We also derive the calculation of the depolarization of the scattered field and the correlation between the co-polarized (same received polarization as the transmitted signal) and de-polarized component of the received scattered signal.

The effects of ground reflections on the elevation pattern of the transmit and receive antennas are accounted by a factor of the form

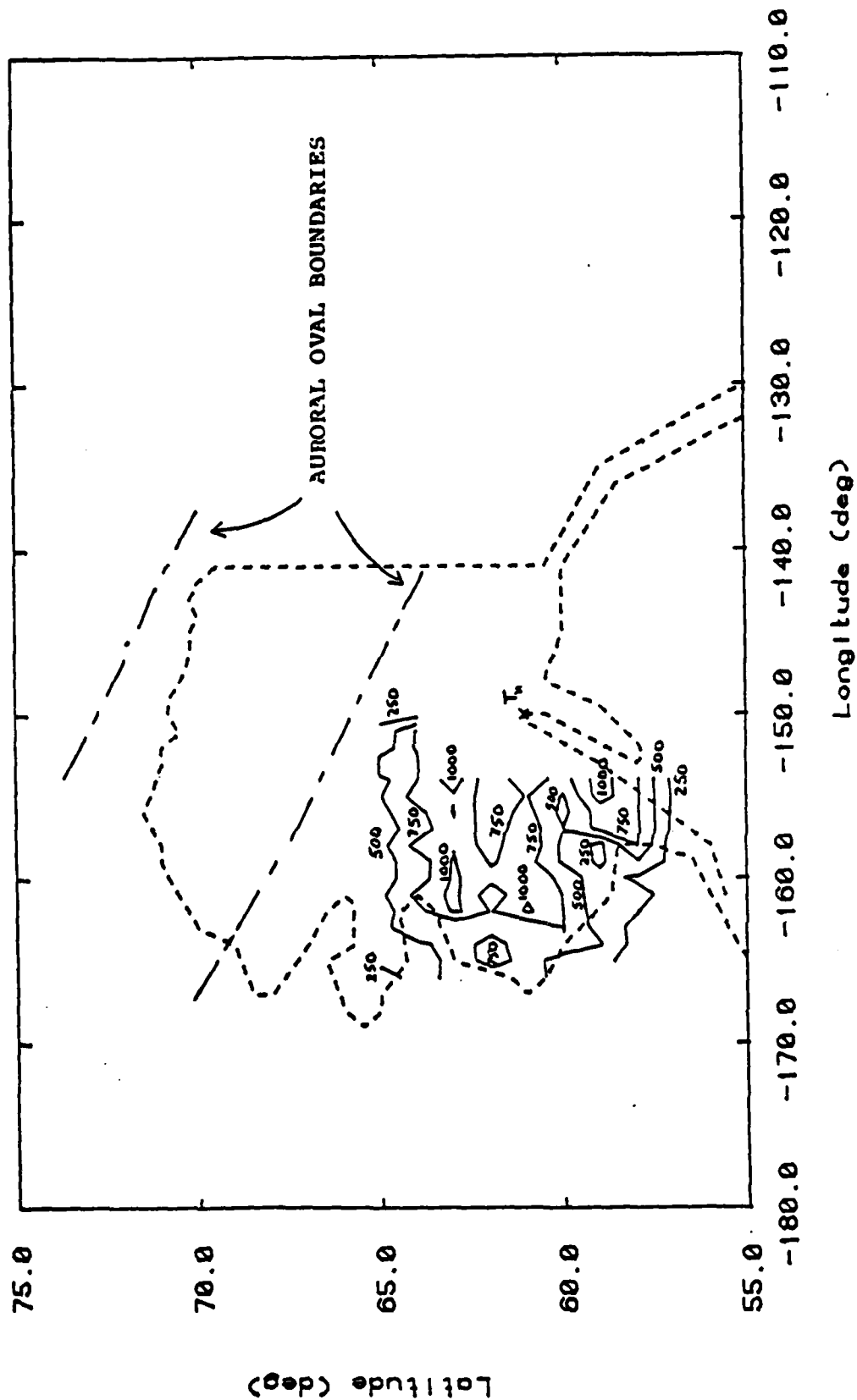


Figure 8 Contours of constant delay spread in microseconds

$$g_{H,V}(h_A, \Delta) = |1 + R_{H,V}(\Delta) \exp\{j4\pi h_A \sin(\Delta)/\lambda\}|^2 \quad (59)$$

where h_A is the height of the antenna, Δ is the elevation take-off angle of the radiated (incident) wave or the elevation angle-of-arrival of the received (scattered) wave, and $R_{H,V}$ is the ground reflection coefficient for horizontal (R_H) or vertical (R_V) polarization which depend on the electrical properties of the ground and the frequency or wavelength λ of the wave. The ground reflection coefficient is given by

$$R_{H,V}(\Delta) = \frac{\sin(\Delta) - z_{H,V}}{\sin(\Delta) + z_{H,V}} \quad (60)$$

$$z_H = \sqrt{\epsilon_g - \cos^2(\Delta) - j60\sigma_g\lambda} \quad (61a)$$

$$z_V = \frac{\sqrt{\epsilon_g - \cos^2(\Delta) - j60\sigma_g\lambda}}{\epsilon_g - j60\sigma_g\lambda} \quad (61b)$$

where ϵ_g and σ_g are the permittivity and conductivity of the ground.

The polarization theory developed in Appendix A and the elevation pattern of Equation (59) have been used to calculate the relative path loss for horizontal transmit and receive polarization, L_{HH} , vertical transmit and receive polarization, L_{VV} , and for horizontal transmit polarization and vertical receive polarization, L_{VH} . The latter is referred to as the depolarized component. Table 1 shows the calculated relative path loss at a frequency of 45 MHz for a transmitter at 61°N and 150°W (Anchorage, Alaska) and a few different receive locations. The calculations assume equal antenna gains and azimuth beamwidths so that

Table 1

POLARIZATION EFFECTS AT 45 MHz

RECEIVER LONGITUDE (deg W)	RECEIVER LATITUDE (deg N)	PATH LENGTH D (km)	RELATIVE PATH LOSS L _{HH} (dB)	RELATIVE PATH LOSS L _{VV} (dB)	RELATIVE PATH LOSS L _{VH} (dB)	DELAY SPREAD T _M (μsec)
162° W	57° N	817	264	261	292	7
162° W	61° N	646	218	214	250	1047
162° W	65° N	750	242	235	282	402
150° W	65° N	445	261	259	310	201
148° W	64° N	349	239	237	309	434
146° W	64° N	392	257	255	314	256
157° W	57° N	598	230	229	271	176
157° W	61° N	377	212	211	254	903
157° W	65° N	567	236	232	275	403

any differences in the path loss are strictly due to the polarization factor $\sin^2\chi$ in the scattering cross-section of the irregularities and ground reflections. A poorly conducting ground is assumed, i.e., $\epsilon_g = 10$ and $\sigma_g = 0.001$ mhos/m. Table 1 also gives the delay spread for each case.

Inspection of Table 1 shows that vertical transmit and receive polarization results in a smaller path loss by a couple of dB. The reason for this is that at high latitudes the scatterers which contribute to most of the received energy are far off the great circle plane because the magnetic fields are nearly vertical. The polarization factor $\sin^2\chi$ has a null on the horizontal plane when the incident wave is horizontally polarized and in the vertical plane for a vertically polarized incident wave. On the other hand, horizontal polarization would be more effective at equatorial latitudes where most of the contributors are near the great circle plane. Table 1 also shows that the depolarized component is 30 to 50 dB weaker than the co-polarized component which implies that polarization diversity would not be an effective way to combat fading if one were to use field-aligned scatter as a VHF communications medium.

3.3 ANTENNA BEAMWIDTH EFFECTS

VHF Meteor Burst Communications systems employ directive antennas in order to achieve a higher effective radiated power. Directivity is achieved mainly in the azimuthal plane. Typical antennas employed are 4-element yagis which have 3 dB beamwidths of 46 degrees [H.E. Green, 1985]. When the elements of the yagi are horizontal, most of the directivity is in the azimuth plane.

Since the field-aligned irregularities which cause auroral scatter are present over a limited geographical area and at specific heights, the beamwidth and direction of the transmit and receive antennas will have a significant effect on strength of the scattered signal.

Table 2 gives the relative path loss and rms delay spread at 45 MHz for various combinations of transmit and receive antenna pointing angles relative to the great circle plane between transmitter and receiver. The transmitter is at a latitude of 61°N and longitude 150°W (Anchorage, Alaska) and the receiver is at a latitude of 61°N and longitude of 162°W (Bethel, Alaska). The great circle distance between these sites is around 646 km. The antennas are assumed to have 3 dB azimuth beamwidths of 45° and only pointing directions north of the great circle plane and towards the other terminal as shown in Figure 9 have been considered. The antennas have also been assumed to have omnidirectional elevation patterns in free space. However, the results include ground reflections which introduce lobing in the elevation pattern and a null for near grazing angles. The relative path loss and rms delay spread for the case in which antennas with omnidirectional azimuth patterns is given in Table 2 for reference purposes also as well as the path loss when ground reflections are ignored (NGR).

When the antennas have azimuth beamwidths of 45°, and they are properly oriented, the increase in path loss relative to an antenna with omnidirectional azimuth pattern is 1 dB. Ignoring the effects of ground reflections results in 17 dB reduction in path loss.

Table 2
ANTENNA AZIMUTH BEAMWIDTH EFFECTS AT 45 MHz

TRANSMIT ANTENNA BORESIGHT DIRECTION γ_T (deg)	RECEIVE ANTENNA BORESIGHT DIRECTION γ_R (deg)	T_A and R_A ANTENNA A_2 3-dB BEAMWIDTH $\Delta\gamma$ (deg)	RELATIVE PATH LOSS L_{HH} (dB)	DELAY SPREAD T_M (μ sec)
90°	60°	45°	220	1078
90°	0°	45°	227	1047
90°	45°	45°	219	1079
75°	45°	45°	220	1023
60°	45°	45°	222	967
45°	45°	45°	226	972
30°	45°	45°	228	992
15°	45°	45°	231	1006
0°	0°	45°	233	1015
0°	0°	OMNI	218	1047
0°	0°	OMNI (No Ground Reflection)	201	1736

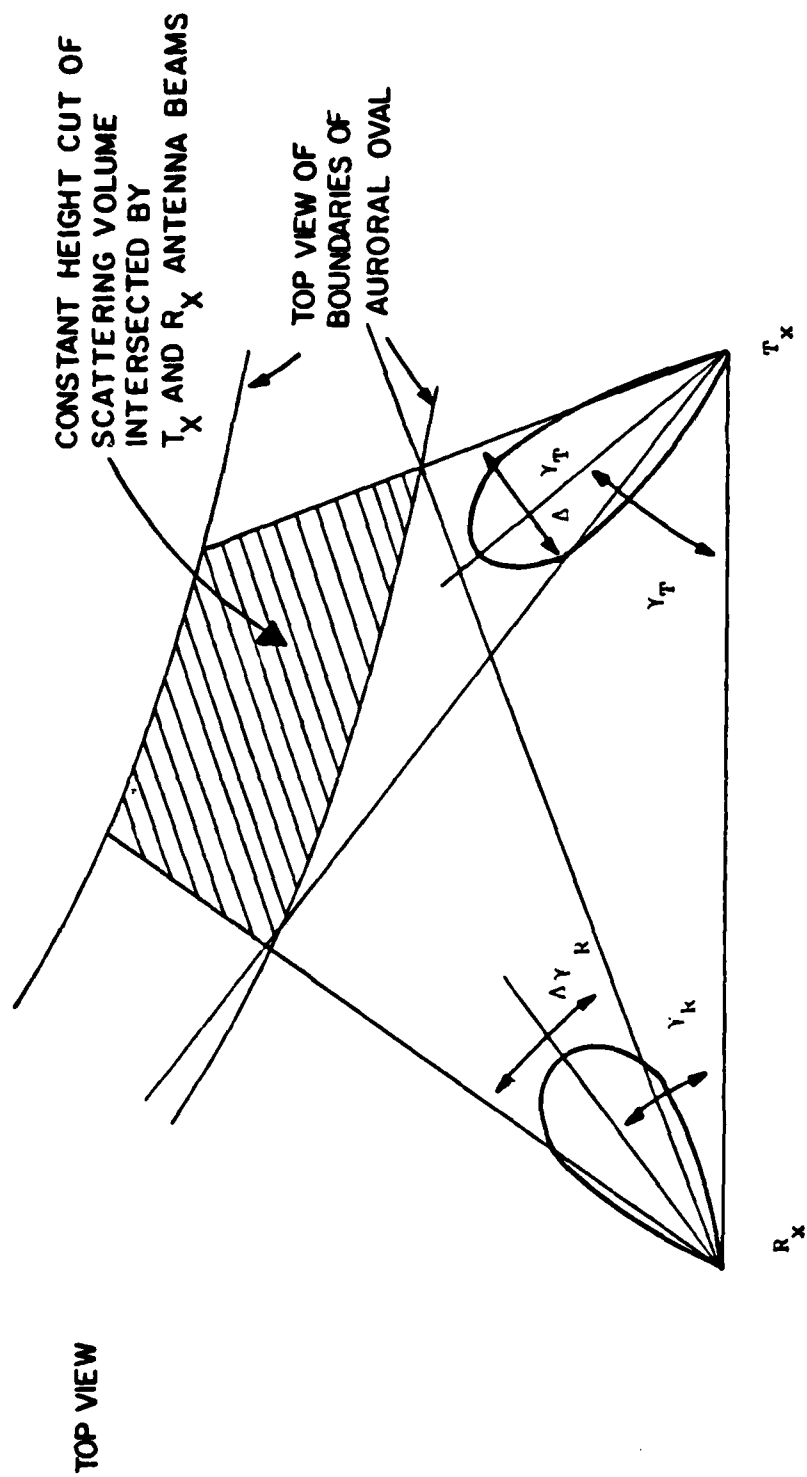


Figure 9 Geometry for calculation of antenna pattern effects

3.4 FREQUENCY DEPENDENCE

The theory of field-aligned scatter developed in Section 2 predicts a path loss with frequency dependence f^{m+2} where m is the power-law dependence of the transverse wavenumber spectrum of the irregularities, all other things being equal such as antenna beamwidth, antenna height in wavelengths and longitudinal outer scale of the irregularities in wavelengths.* For a power law dependence of $m = 4$ and fixed antenna gains, the path loss should increase 18 dB every time the frequency is doubled. However, for a fixed longitudinal outer scale of the irregularities the scatter is more specular at higher frequencies resulting in greater frequency dependence than that predicted by the power law f^{m+2} . The effect of the anisotropy and resulting specularity on the frequency dependence of field-aligned scatter is shown in Table 3 where we give the relative path loss and the delay spread at 30, 45, 60 and 90 MHz for the same 646 km path of Section 3.3. The antenna height assumed was 0.6λ for all frequencies so that the elevation pattern lobing effects is similar at all frequencies. The deviation in path loss from the predicted 18 dB per octave for a power law $m = 4$ is also listed in the table.

4. SUMMARY AND CONCLUSIONS

A theory for calculating and predicting the characteristics of VHF signals scattered by ionization irregularities in the ionosphere has been developed. The theory is applicable for prediction of the effects of VHF auroral scatter as well as the VHF 'bomb mode' of propagation which is known to occur after a high-altitude (100-500 km) nuclear explosion. In order for the theory

* NOTE: The f^{m+2} frequency dependence also assumes that the ratio of the transverse outer, L_T , to the wavelength is much larger than 1.

Table 3
FREQUENCY EFFECTS

OPERATING FREQUENCY (MHz)	RELATIVE PATH LOSS L_{HH} (dB)	ADDITIONAL PATH LOSS ABOVE 18 dB/OCTAVE (dB)	DELAY SPREAD T_M (μsec)
30	206.3	-	1081
45	218.6	1.7	1079
60	227.4	3.1	1074
90	240.1	5.2	1067

to be useful as a prediction tool, data concerning the electron density fluctuations and the outer scales of the irregularities along and transverse to the earth's magnetic field is needed. In order to predict the rapidity of the fading, data regarding the velocity at which the irregularities move across and transverse to the earth's magnetic field lines is required.

Some of these data can be obtained from measurements of the strength of field-aligned scatter signals as well as their fading rate and multipath spread provided the critical frequency of the scattering layer where the irregularities are present and the absorption loss in the D-region of the ionosphere are measured simultaneously.

The theoretical model has been applied to investigate auroral scatter at VHF. In particular the results obtained assuming that field aligned irregularities occur at E-layer heights in a band of latitudes coinciding with the auroral oval predict the following:

- i) Auroral scatter is aspect sensitive with stronger signals occurring on east-west paths although, it is also possible to observe auroral scatter on north-south paths provided the terminals are both south of the scattering region.
- ii) Delay spreads as large as one millisecond are predicted on east-west paths provided the irregularities occupy a region extending from 65°N to 71°N in geomagnetic coordinates and the antenna patterns are sufficiently broad to illuminate most of the scattering region.

- iii) Vertically polarized antennas result in large scattered signal strengths at high latitudes than horizontally polarized antennas (by 2-4 dB) because the main scatterers are well off the great circle plane.
- iv) The depolarized component of the scattered signal is 30-40 dB weaker than the co-polarized component so that polarization diversity is of no use to combat fading.
- v) The strength of field aligned scatter decreases with frequency faster than the power law dependence f^{-6} . This is due to the fact that the scatter is more specular at higher frequencies so that fewer scatterers contribute to the total received signal.

REFERENCES

- Bailey, D.K., R. Bateman, and R.C. Kirby (1955), "Radio transmission at VHF by scattering and other processes in the lower ionosphere", *Proc. IRE*, V. 43, pp. 1181-1230.
- Booker, H.G. (1956), "A theory of scattering by non-isotropic irregularities with application to radar reflections from the aurora", *J. Atmos. Terr. Physics*, V. 8, pp. 204-221.
- Collins, C. and P.A. Forsyth (1959), "A bistatic radio investigation of auroral ionization", *J. Atmos. Terr. Physics*, V. 13, pp. 315-345.
- Ferguson, J.A. (1981), "The role of ionospheric irregularities in transequatorial propagation at VHF", in Effect of the Ionosphere on Radiowave Systems, J.M. Goodman Ed., U.S. Government Printing Office, Washington D.C., pp. 372-380.
- Fremouw and Lansinger (1981), "Recent high-latitude improvements in a computer-based scintillation Model", in Effect of the Ionosphere on Radiowave Systems, J.M. Goodman Ed., U.S. Government Printing Office, Washington, D.C., pp. 141-154.
- Gassmann, G.L. (1973), "Analog model 1972 of the arctic ionosphere", Tech. Report AFCE-TR-73-0151, Air Force Cambridge Research Labs.
- Green, H.E. (1985), "Design of Yagi-Uda arrays", *IEEE Antennas and Propagation Society Newsletter*, pp. 11-13.
- Malaga, A. (1981), "A Global Model for Wideband HF Skywave Propagation", in Effect of the Ionosphere on Radiowave Systems, J.M. Goodman Ed., U.S. Government Printing Office, Washington, D.C., pp. 553-564.
- Stathacopoulos, A.D. and G.H. Barry (1974), "Geometric Considerations in the design of communications circuits using field-aligned ionospheric scatter", *Radio Science*, V. 9, No. 11, pp. 1021-1024.
- Yang, C. and K.C. Yeh (1984), "Effects of Multiple Scattering and Fresnel Diffraction on Random Volume Scattering", *IEEE Trans. on Antennas and Propagation*, V. AP-32, No. 4, pp. 347-355.

APPENDIX A

POLARIZATION EFFECTS IN FIELD-ALIGNED SCATTER

A.1 INTRODUCTION

In this appendix we develop the theory necessary to investigate the role played by the polarization of radio waves in the scattering from field-aligned irregularities. In particular we would like to determine whether horizontal or vertical polarization is more suitable for field-aligned scatter, how much depolarization there is, and if the depolarized component is of the same order of magnitude as the co-polarized component whether the co-polar and depolarized component fade independently or not.

A.2 DEPOLARIZATION THEORY FOR FIELD-ALIGNED SCATTER

In order to determine the role played by polarization in the scattering from field-aligned irregularities we start from the basic equation for the field scattered by a dielectric particle (perturbation).

Field-aligned irregularities can be modeled as perturbations of the refractive index of the ionosphere. Thus if $n_0(z)$ is the refractive index of the background ionosphere and $\Delta n(\vec{r})$ is the perturbation of the refractive index due to the field-aligned irregularities, then the scattered field is given by [Ishimaru, 1978]

$$\vec{E}_s(\vec{r}) = \frac{k^2}{2\pi} \int_V [\hat{u}_0 \times (\vec{E}(\vec{r}') \times \hat{u}_0)] \Delta n(\vec{r}') \frac{e^{jk|\vec{r}-\vec{r}'|}}{|\vec{r}-\vec{r}'|} dV' \quad (A.1)$$

where $\vec{E}(\vec{r})$ is the total electric field inside the scattering volume V and \hat{u}_0 is a unit vector in the direction of the scattered field, i.e.,

$$\hat{u}_0(\bar{r}') = \frac{\bar{r} - \bar{r}'}{|\bar{r} - \bar{r}'|} \quad (\text{A.2})$$

Equation (A.1) is an exact solution of Maxwell's equations in terms of the field $\bar{E}(\bar{r}')$ inside the scattering volume and the perturbation of the refractive index $\Delta n(\bar{r}')$. The exact field inside the scattering volume is not known and the perturbation of the refractive index is a random function of the location within the scattering volume. An approximate solution can be obtained if we replace the field inside the scattering volume by the incident field $\bar{E}_i(\bar{r}')$ and assume uncorrelated scatter. The latter assumption implies that the field scattered by irregularities spaced by more than the 'correlation distance' of the perturbation of the refractive index is uncorrelated. Therefore we can divide the scattering volume into sub-volumes of dimensions of the order of the 'correlation distance' of the refractive index perturbation. The total average scattered power would then be equal to the sum of the average power scattered by irregularities occupying each sub-volume. This can be expressed mathematically as

$$\bar{E}_s(\bar{r}) = \sum_m \frac{k^2}{2\pi} \int_{\Delta V_m} [\hat{u}_{0m} \times (\bar{E}_i(\bar{r}_m) \times \hat{u}_{0m})] \Delta n(\bar{r}_m) \frac{e^{-jk|\bar{r} - \bar{r}_m|}}{|\bar{r} - \bar{r}_m|} dV_m \quad (\text{A.3})$$

where the incident field due to a source at \bar{r}_0 with polarization vector \hat{e}_i is given by

$$\bar{E}_i(\bar{r}_m) = \frac{e^{-jk|\bar{r}_0 - \bar{r}_m|}}{|\bar{r}_0 - \bar{r}_m|} \hat{e}_i \quad (A.4)$$

Note that (A.3) reduces to (A.1) in the limit as $\Delta V_m \rightarrow 0$. We have chosen to express the integral (A.1) as a discrete sum of integrals to facilitate the derivation and interpretation of the results that follow.

When the source and observation points are in the far field of the scatterer at \bar{r}_m we approximate the wave functions as

$$\frac{e^{-jk|\bar{r} - \bar{r}_m|}}{|\bar{r} - \bar{r}_m|} = \frac{\exp[-jk(R_{rm} - \bar{r}_m \cdot \hat{u}_{0m})]}{R_{rm}} \quad (A.5)$$

$$\frac{e^{-jk|\bar{r}_0 - \bar{r}_m|}}{|\bar{r}_0 - \bar{r}_m|} = \frac{\exp[-jk(R_{tm} + \bar{r}_m \cdot \hat{u}_{im})]}{R_{tm}} \quad (A.6)$$

$$\hat{u}_{0m} = \frac{\bar{r} - \bar{r}_{m0}}{|\bar{r} - \bar{r}_{m0}|} = \frac{\bar{r} - \bar{r}_{m0}}{R_{rm}} \quad (A.7)$$

$$\hat{u}_{im} = \frac{\bar{r}_{m0} - \bar{r}_0}{|\bar{r}_{m0} - \bar{r}_0|} = \frac{\bar{r}_{m0} - \bar{r}}{R_{tm}} \quad (A.8)$$

where \bar{r}_{m0} are the coordinates of the center of the m^{th} sub-volume.

Substitution of (A.5)-(A.8) in Equation (A.3) leads to

$$\bar{E}_s = \sum_m \frac{k^2}{2\pi} \frac{\exp[-jk(R_{tm} + R_{rm})]}{R_{tm} R_{rm}} \hat{e}_{sm} \int_{\Delta V_m} \Delta n(\bar{r}_m) \exp[jk\bar{r}_m \cdot \hat{u}_{sm}] dV_m \quad (A.9)$$

where

$$\hat{e}_{sm} = \hat{u}_{0m} \times (\hat{e}_{im} \times \hat{u}_{0m}) = \sin \chi_m \quad (A.10)$$

$$\hat{u}_{sm} = \hat{u}_{0m} - \hat{u}_{im} \quad (A.11)$$

The vector \hat{e}_{sm} is the polarization of the wave scattered by the m^{th} irregularity and is a function of the incident wave polarization and the scattered wave direction of propagation. The average received power is proportional to the received field intensity defined as

$$I_s = \overline{|E_s|^2} \\ = \sum_m \sum_n \frac{k^4}{n(2\pi)^2} \frac{\sin \chi_m \sin \chi_n}{R_{tm} R_{tn} R_{rm} R_{rn}} \int_{\Delta V_m} \int_{\Delta V_n} \overline{\Delta n(\bar{r}_m) \Delta n(\bar{r}_n')} \exp[jk\hat{u}_{sm} \cdot (\bar{r}_m - \bar{r}_n')] dV_m dV_n'$$

which by virtue of the uncorrelated scatter assumption

$$\overline{\Delta n(\bar{r}_m) \Delta n(\bar{r}_n')} = \delta_{nm} \overline{\Delta n(\bar{r}_m) \Delta n(\bar{r}_m')} \quad (A.12)$$

becomes

$$I_s = \sum_m \frac{k^4}{(2\pi)^2} \frac{\sin^2 \chi_m}{R_{tm}^2 R_{rm}^2} S(k\hat{u}_{sm}) \Delta V_m \quad (A.13)$$

where $S(\vec{K})$ is the three-dimensional wavenumber spectrum of the irregularities, i.e.,

$$S(\vec{K}) = \int_{\Delta V} B(\vec{r}) e^{j\vec{K} \cdot \vec{r}} dV \quad (A.14)$$

and

$$B(\vec{r}) = \overline{\Delta n(\vec{r} + \vec{r}_0) \Delta n(\vec{r}_0)} \quad (A.15)$$

In the limit as $\Delta V_m \rightarrow 0$, Equation (A.13) reduces to the solution for the average power scattered by a random medium presented in Section 2 of this report.*

To determine depolarization effects we go back to Equation (A.9) and express the polarization of the wave incident and scattered by each irregularity as the sum of two orthogonal polarizations denoted as horizontal and vertical polarization respectively. We also assume the axis of symmetry of the field-aligned

* NOTE: The equation for the average scattered power given in Section 2, Equation (14) includes the the effects of the antenna patterns and absorption loss which have been omitted in this appendix to simplify the discussion.

irregularities (magnetic field line) to be the z-axis as shown in Figure A.1. Then the horizontal polarization component E_ϕ is defined as the field component on the x-y plane which is normal to the axis of symmetry. Note that when the scattering region is near the magnetic pole this plane is nearly parallel to the surface of the earth so that the E_ϕ field component nearly coincides with the horizontal polarization as it would be defined on a coordinate system whose reference point is the transmitter or receiver location. However this is no longer true when the scattering region is near the magnetic equator. In this case a coordinate transformation must be done to convert from polarizations in the scattering volume to polarizations in the transmitter or receiver coordinate system.

In the scattering volume coordinate system of Figure A.1, the vertical and horizontal components of the scattered field can be expressed in terms of the vertical and horizontal components of the incident field as *

$$\begin{bmatrix} E_{s\theta}^m \\ E_{s\phi}^m \end{bmatrix} = \frac{k^2 e^{-jk(R_{tm} + R_{rm})}}{2\pi R_{tm} R_{rm}} \begin{bmatrix} f_{11}^m & f_{12}^m \\ f_{21}^m & f_{22}^m \end{bmatrix} \begin{bmatrix} e_{i\theta}^m \\ e_{i\phi}^m \end{bmatrix} \quad (A.16)$$

where the f_{ij}^m are complex scattering amplitudes given by

* NOTE: In this appendix we use suffixes θ and ϕ to denote the parallel and perpendicular components of the incident field polarization rather than geomagnetic latitude and longitude.

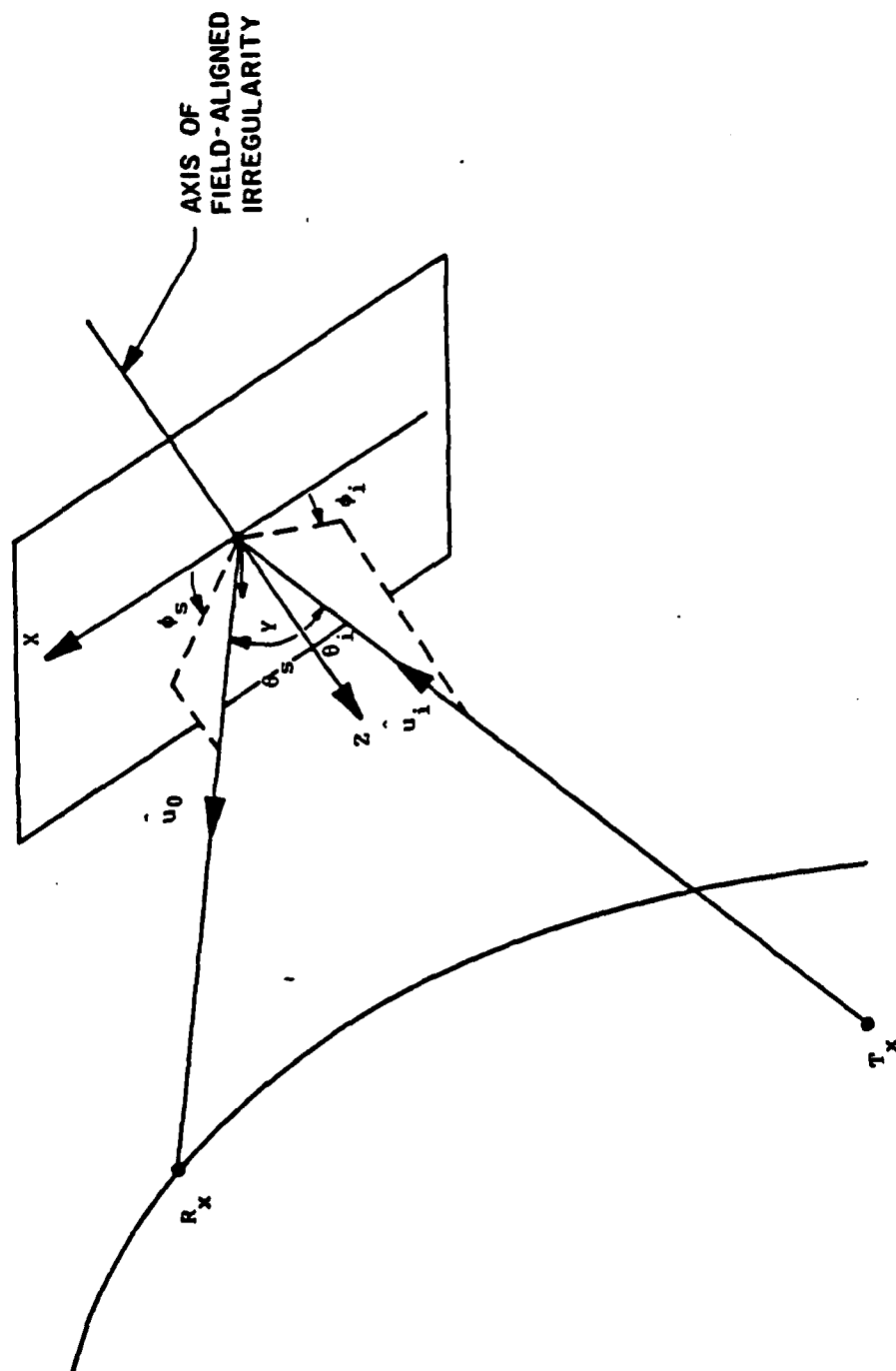


Figure A-1 Geometry for Calculation of Polarization Effects in Field-Aligned Scatter

$$f_{ij}^m = \alpha_{ij}^m \int_{\Delta V_m} \Delta n(\bar{r}_m) \exp[jk \hat{u}_{sm} \cdot \bar{r}_m] dV_m, \quad i, j = 1, 2 \quad (A.17)$$

$$\begin{aligned} \alpha_{11}^m &= \hat{e}_{s\theta}^m \cdot [\hat{u}_{0m} \times (\hat{e}_{i\theta}^m \times \hat{u}_{0m})] \\ &= \sin\theta_{im} \sin\theta_{sm} + \cos\theta_{im} \cos\theta_{sm} \cos(\phi_{im} - \phi_{sm}) \end{aligned} \quad (A.18a)$$

$$\begin{aligned} \alpha_{12}^m &= \hat{e}_{s\theta}^m \cdot [\hat{u}_{0m} \times (\hat{e}_{i\phi}^m \times \hat{u}_{0m})] \\ &= -\cos\theta_{sm} \sin(\phi_{im} - \phi_{sm}) \end{aligned} \quad (A.18b)$$

$$\begin{aligned} \alpha_{21}^m &= \hat{e}_{s\phi}^m \cdot [\hat{u}_{0m} \times (\hat{e}_{i\theta}^m \times \hat{u}_{0m})] \\ &= \cos\theta_{im} \sin(\phi_{im} - \phi_{sm}) \end{aligned} \quad (A.18c)$$

$$\begin{aligned} \alpha_{22}^m &= \hat{e}_{s\phi}^m \cdot [\hat{u}_{0m} \times (\hat{e}_{i\phi}^m \times \hat{u}_{0m})] \\ &= \cos(\phi_{im} - \phi_{sm}) \end{aligned} \quad (A.18d)$$

The polar angles (θ_{im}, ϕ_{im}) and (θ_{sm}, ϕ_{sm}) for the incident and scattered waves, respectively, are defined in Figure A.1.

The horizontal and vertical components of the total scattered field in the coordinates of the receive location can then

be expressed in terms of the horizontal and vertical components of the radiated field as

$$\begin{bmatrix} E_{sv} \\ E_{sh} \end{bmatrix} = \sum_m C_m H(\hat{k}u_{sm}) \begin{bmatrix} \cos\beta_r & \sin\beta_r \\ -\sin\beta_r & \cos\beta_r \end{bmatrix} \begin{bmatrix} \alpha_{11}^m & \alpha_{12}^m \\ \alpha_{21}^m & \alpha_{22}^m \end{bmatrix} \begin{bmatrix} \cos\beta_t & \sin\beta_t \\ -\sin\beta_t & \cos\beta_t \end{bmatrix} \begin{bmatrix} E_{iv} \\ E_{ih} \end{bmatrix}$$

(A.19)

where

$$C_m = \frac{k^2 \exp[-jk(R_{tm} + R_{rm})]}{2\pi R_{tm} R_{rm}} \Delta V_m \quad (A.20)$$

$$H(\hat{k}u_{sm}) = \frac{1}{\Delta V_m} \int_{\Delta V_m} \Delta n(\vec{r}_m) \exp(jk\hat{n}_{sm} \cdot \vec{r}_m) dV_m \quad (A.21)$$

and the angles β_t and β_r , which describe the coordinate transformations for the transmitter and receiver respectively, are to be determined. At high latitudes where the magnetic field lines are nearly perpendicular, $\beta_t \approx 0$ and $\beta_r \approx 0$.

The three matrices in (A.19) describe depolarization due to anisotropic field-aligned irregularities. When the irregularities are isotropic the total received field results mostly from contributions due to scatterers which lie on the great circle plane between transmitter and receiver, i.e., scatterers for which $\phi_{im} - \phi_{sm} = \pi$ and hence $\alpha_{12}^m = \alpha_{21}^m = 0$ (from A.18). Also since the scatterers have no axis of symmetry the coordinate systems

can be chosen so that $\beta_t = \beta_r = 0$ and we get the result that isotropic scatterers (on the great circle plane) do not depolarize the incident wave. The depolarization of the waves scattered by isotropic irregularities off the great circle plane is small and can be ignored in practical applications. Also, the scattering amplitude $\alpha_{11}^m < \alpha_{22}^m$ when the scatterers are on the great circle plane so that horizontal polarization will in general result in a slightly stronger signal than vertical polarization.

However when the irregularities are anisotropic, the strongest contributors to the total received field are not necessarily on the great-circle plane so that depolarization effects can be significant. The fact that the received field is depolarized does not, however, imply that the two orthogonal polarizations fade independently as will be seen from the following discussions. Also the scattering amplitudes for horizontal polarization are not necessarily greater than for vertical polarization since the main contributors are not necessarily on the great circle plane.

A.3 STATISTICS OF THE DEPOLARIZED SCATTERED FIELD

In order to determine which polarization yields a stronger signal and whether the cross polarized components of the received field fade independently we need to evaluate the average received power for each polarization and the covariance (correlation) for the two polarizations, i.e., we need to evaluate the averages $\overline{|E_{sv}|^2}$, $\overline{|E_{sh}|^2}$ and $\overline{E_{sv}E_{sh}^*}$ where the averaging is over the statistics of the refractive index perturbation. These can be expressed in terms of the incident power in matrix form as

$$\begin{bmatrix} \overline{|E_{sv}|^2} \\ \overline{|E_{sh}|^2} \\ \overline{E_{sv}E_{sh}^*} \end{bmatrix} = \sum_m \frac{\sigma_{sm}}{R_{tm}^2 R_{rm}^2} \Delta V_m \begin{bmatrix} G_{11}^m & G_{12}^m \\ G_{21}^m & G_{22}^m \\ G_{31}^m & G_{32}^m \end{bmatrix} \begin{bmatrix} |E_{iv}|^2 \\ |E_{ih}|^2 \end{bmatrix} \quad (A.22)$$

where use has been made of the uncorrelated scatter assumption. The function σ_{sm} is the scattering cross section per unit volume of the refractive index fluctuations to be defined below and the 3×2 scattering matrix G^m is real with elements given by (from Equation A.19)

$$G_{11}^m = [\cos\beta_r(\alpha_{11}^m \cos\beta_t - \alpha_{12}^m \sin\beta_t) + \sin\beta_r(\alpha_{21}^m \cos\beta_t - \alpha_{22}^m \sin\beta_t)]^2 \quad (A.23a)$$

$$G_{12}^m = [\cos\beta_r(\alpha_{11}^m \sin\beta_t + \alpha_{12}^m \cos\beta_t) + \sin\beta_r(\alpha_{21}^m \sin\beta_t + \alpha_{22}^m \cos\beta_t)]^2 \quad (A.23b)$$

$$G_{21}^m = [-\sin\beta_r(\alpha_{11}^m \cos\beta_t - \alpha_{12}^m \sin\beta_t) + \cos\beta_r(\alpha_{21}^m \cos\beta_t - \alpha_{22}^m \sin\beta_t)]^2 \quad (A.23c)$$

$$G_{22}^m = [-\sin\beta_r(\alpha_{11}^m \sin\beta_t + \alpha_{12}^m \cos\beta_t) + \cos\beta_r(\alpha_{21}^m \sin\beta_t + \alpha_{22}^m \cos\beta_t)]^2 \quad (A.23d)$$

$$G_{31}^m = \sqrt{G_{11}^m G_{21}^m} \quad (A.23e)$$

$$G_{32}^m = \sqrt{G_{12}^m G_{22}^m} \quad (A.23f)$$

The scattering cross-section per unit volume is defined as

$$\sigma_{sm} = \frac{k^4}{(2\pi)^2} S(\hat{k}u_{sm}) \quad (A.24)$$

where $S(\hat{k}u_{sm})$ is the 3-dimensional wavenumber spectrum of the irregularities defined in Equation (A.14) whose argument depends on the incident and scattered angles. In the coordinates of Figure A.1 the vector \hat{u}_{sm} is given by

$$\begin{aligned} \hat{u}_{sm} = & (\sin\theta_{im}\cos\phi_{im} - \sin\theta_{sm}\cos\phi_{sm})\hat{x} + (\sin\theta_{im}\sin\phi_{im} - \sin\theta_{sm}\sin\phi_{sm})\hat{y} \\ & + (\cos\theta_{im} - \cos\theta_{sm})\hat{z} \end{aligned} \quad (A.25)$$

In the case of anisotropic irregularities with axis of symmetry along the z-axis, we can rewrite (A.24) as

$$\sigma_{sm} = \frac{k^4 \overline{\Delta n^2}}{(2\pi)^2} S_T(K_{Tm}) S_L(K_{Lm}) \quad (A.26)$$

where $S_T(\cdot)$ and $S_L(\cdot)$ are the normalized transverse and longitudinal wavenumber spectra defined in Section 2 of this report and $\overline{\Delta n^2}$ is the mean square refractive index fluctuation. The arguments of these spectra are given by (in terms of the notation given here)

$$K_{Lm} = k(\cos\theta_{im} - \cos\theta_{sm}) \quad (A.27)$$

$$K_{Tm}^2 = k^2[(\sin\theta_{im}\cos\phi_{im} - \sin\theta_{sm}\cos\phi_{sm})^2 + (\sin\theta_{im}\sin\phi_{im} - \sin\theta_{sm}\sin\phi_{sm})^2]$$

From Equations (A.22) and (A.23) we can see that the covariance of the two orthogonal polarizations, $E_{sv}E_{sh}^*$, does not vanish in general since the matrix elements G_{31}^m and G_{32}^m are not zero for all m . Therefore the fading (statistics) of the two polarizations is correlated. The correlation between the two polarizations is given by

$$\rho_{vh} = \frac{E_{sv}E_{sh}^*}{\sqrt{|E_{sv}|^2|E_{sh}|^2}} \quad (A.28)$$

Some decorrelation will occur whenever different scatterers within the scattering volume contribute most of the power received on each polarization. For example if the transmitted signal is horizontally polarized and most of the contributions to the received horizontal polarization is due to the $m = M$ scattering sub-volume while most of the received vertical polarization is due to the $m = N$ scattering sub-volume, then the correlation between the two polarizations is given by

$$\rho_{vh} = \frac{P_M G_{32}^M + P_N G_{32}^N}{\sqrt{P_N G_{12}^N P_M G_{22}^M}} \quad (A.29)$$

where P_N and P_M are the total power scattered by the N^{th} and M^{th} scatterers and $G_{12}^M \ll G_{12}^N$, $G_{22}^N \ll G_{22}^M$. Using Equations (A.23e) and (A.23f) to substitute for G_{32}^N and G_{32}^M in (A.29) we get

$$\rho_{vh} = \sqrt{\frac{P_M G_{12}^M}{P_N G_{12}^N}} + \sqrt{\frac{P_N G_{22}^N}{P_M G_{22}^M}} \ll 1 \quad (\text{A.30})$$

provided $P_N = P_M$.

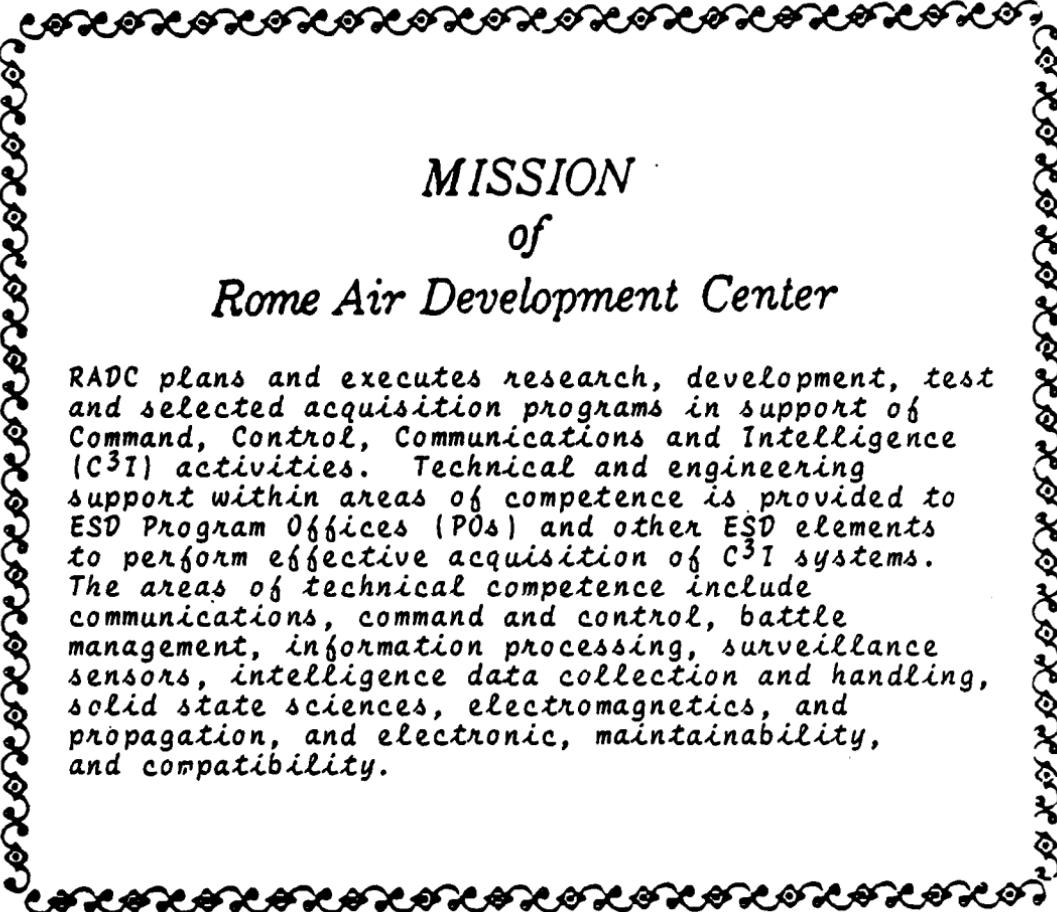
A sufficient condition for uncorrelated polarization fading is that the effective scattering volumes for the two polarizations be different, a condition that will not be met in most cases unless the antenna patterns for the polarizations are significantly different, i.e., they illuminate different parts of the scattering volume.

A.4 SUMMARY

A theory for analyzing polarization effects on field aligned scatter has been developed. The scattering matrix G defined in Equations (A.22) and (A.23) can be used along with the theory of Section 2 of this report to calculate the effects of polarization. The effects of different antenna patterns for each polarization can be analyzed by multiplying the elements of the scattering matrix G with the appropriate antenna patterns.

REFERENCES

- A. Ishimaru, (1978) Wave Propagation and Scattering in Random Media, V1 and V2, Academic Press, New York, 1978.



*MISSION
of
Rome Air Development Center*

RADC plans and executes research, development, test and selected acquisition programs in support of Command, Control, Communications and Intelligence (C³I) activities. Technical and engineering support within areas of competence is provided to ESD Program Offices (POs) and other ESD elements to perform effective acquisition of C³I systems. The areas of technical competence include communications, command and control, battle management, information processing, surveillance sensors, intelligence data collection and handling, solid state sciences, electromagnetics, and propagation, and electronic, maintainability, and compatibility.

END

12-86

DTIC